浙江大学高校教师专业技术高级职务申报表

姓名	万灵书
单位	高分子科学与工程学系
所在学科	高分子化学与物理
现专业技术职务	副教授
申请专业技术职务	教授
申请研究生招生资格	不申请(已具有相应资格)
联系电话	13606605693
Email	lswan@zju.edu.cn

填报日期：2015年 9月

一、基本情况			
姓名	万灵书	性别	男
出生年月	19800617	国籍	中国
兼任党政职务		现专业技术职务	副教授
任职时间	20091228	所在二级学科	高分子化学与物理
申请研招资格	不申请(已具有相应资格)	申请专业技术职务	教授
现工作单位	高分子科学与工程学系		
从事专业及专长	高分子化学与物理/高分子分离膜		
联系电话	13606605693	Email	lswan@zju.edu.cn
最后学历、毕业学校、所学专业、学位及取得时间、导师姓名	博士、浙江大学、高分子化学与物理专业、理学博士、2007年6月、导师徐志康教授。		
主要学术兼职	[1] Int. J. Polym. Sci.客座编辑(SCI期刊，影响因子1.322)。 [2] 美国物理学会会员。		
个人简历（要求从大学开始，采用时间倒序方式填写，时间不间断）			
“学历进修经历”填写格式：自何年月至何年月，在何地，何学校（单位），何专业，学习、进修，导师;			
学习进修经历	200209–200706：浙江大学，高分子化学与物理，硕博连读学习，导师徐志康教授 199809–200206：南京工业大学，高分子化工，本科学习		

“工作经历”填写格式：自何年月至何年月，在何地、何学校（系所）、何单位任职，任何职（海外职位英文表述）；

工作经历	201304–至今：浙江大学，高分子化学与物理专业，博士生招收资格 201301–至今：浙江大学，求是青年学者 201209–201309：University of Chicago，Institute for Molecular Engineering，Postdoctoral Researcher，Prof. Paul F. Nealey 201005–至今：浙江大学，高分子化学与物理专业，硕士生导师 200912–至今：浙江大学，高分子科学与工程学系，副教授 200709–200912：浙江大学，高分子科学与工程学系，讲师 200707–200906：浙江大学，材料科学与工程博士后流动站，师资博士后，合作导师徐志康教授

二、申请人标志性工作(不超过300字)

以具有可控表面性质的孔径单分散分离膜为目标，在聚合物多孔膜及其表界面领域首创基于呼吸图法的孔径单分散分离膜，建立了多层次结构调控方法，实现了精密分离；拓展了孔径单分散膜制备的界面理论，发现了膜表面浸润性转变规律，提出了区域选择性界面功能化新策略。近五年在J Am Chem Soc等期刊以通讯作者发表SCI论文27篇，影响因子总和137.38、篇均5.088，他引239次，H指数29，所有论文总他引1811次；获发明专利授权18项；以第一完成人获浙江省高等学校科研成果一等奖等奖励；应邀在ChemComm撰写综述论文，担任SCI期刊Int J Polym Sci的客座编辑，在学术会议做邀请报告和分会主持人；获国家自然科学基金委优秀青年科学基金资助。

三、申请人任现职以来近五年主要业绩

3.1 教学与人才培养情况

1、共开设课程4门，课程教学时数共计223学时。其中本科生课程1门，课程教学时数112学时。开课情况如下：

(填写格式：教学年度，课程名称，授课对象，学生数，学时数，考核结果)

201010-201012	高分子化学实验	本科生	91	16	
201009-201011	高聚物结构近代分析技术(I)	研究生	84	20	
201110-201112	高分子化学实验	本科生	103	16	良
201109-201111	高聚物结构近代分析技术(I)	研究生	78	20	
201310-201312	高分子化学实验	本科生	92	24	良
201309-201311	高聚物结构近代分析技术(I)	研究生	83	20	
201410-201412	高分子化学实验	本科生	94	24	良
201409-201411	高聚物结构近代分析技术(I)	研究生	78	24	
201510-201512	高分子化学实验	本科生	48	24	
201509-201511	高分子科学前沿	研究生	24	15	
201509-201511	聚合物结构表征原理	研究生	72	20	

2、指导本科生毕业论文(设计)13人(请列出姓名、专业、年级)

(填写格式：姓名，专业，年级)

杨 轩	高分子材料与工程	2007
李青莲	高分子材料与工程	2007
张 菁	高分子材料与工程	2008
姜 婵	高分子材料与工程	2008

邓　然	高分子材料与工程	2009
杨　武	高分子材料与工程	2009
王黎阳	高分子材料与工程	2009
肖文达	高分子材料与工程	2009
曹　博	高分子材料与工程	2010
吴柏衡	高分子材料与工程	2010
汤　文	高分子材料与工程	2011
陈森河	高分子材料与工程	2011
易铭翰	高分子材料与工程	2011

3、指导研究生8名，协助指导博士生2人(请列出研究生姓名、专业、年级)

(填写格式：研究生姓名，专业，年级)

柯蓓蓓	高分子化学与物理直博生	2006（协助指导）
金　晶	高分子化学与物理硕士生	2008（协助指导）
朱凉伟	高分子化学与物理硕士生	2011
欧　洋	高分子化学与物理直博生	2011（协助指导）
俞　翔	高分子化学与物理硕士生	2012
吴联巍	高分子化学与物理硕士生	2013
朱凉伟	高分子化学与物理提前攻博	2014
吴柏衡	高分子化学与物理直博生	2014
仲启智	高分子化学与物理硕士生	2014
陈森河	高分子化学与物理硕士生	2015

3.2 代表性论文、著作情况

共发表论文59篇。其中作为第一作者或通讯作者27篇，请按照您认为最具代表性、重要性或影响力的顺序列出：(不超过15篇)

(填写格式：所有作者姓名（通讯作者名字上用“*”标示），论文题目，发表期刊名称，出版年月，卷，期，起止页码，检索情况，期刊影响因子，他引次数)

[1] 万灵书*、李隽巍、柯蓓蓓、徐志康，Ordered microporous membranes templated by breath figures for size-selective separation，Journal of the American Chemical Society，201201，134，1，95-98，SCI，IF=12.113，他引53次。

[2] 万灵书*、朱凉伟、欧洋、徐志康，Multiple interfaces in self-assembled breath figures，Chemical Communications，201403，50，31，4024-4039，SCI，IF=6.834，他引22次。

[3] 万灵书*、李青莲、陈鹏程、徐志康，Patterned biocatalytic films via one-step self-assembly，Chemical Communications，201204，48，37，4417-4419，SCI，IF=6.834，他引13次。

[4] 欧洋、吕常江、俞维、毛峥伟、万灵书*、徐志康，Fabrication of perforated isoporous membranes via a transfer-free strategy: enabling high-resolution separation of cells，ACS Applied Materials & Interfaces，201411，6，24，22400-22407，SCI，IF=6.723，他引5次。

[5] 万灵书*、吕劼、柯蓓蓓、徐志康，Facilitated and site-specific assembly of functional polystyrene microspheres on patterned porous films，ACS Applied Materials & Interfaces，201012，2，12，3759-3765，SCI，IF=6.723，他引16次。

[6] 朱凉伟、杨武、欧洋、万灵书*、徐志康，Synthesis of core cross-linked star polystyrene with functional end groups and self-assemblies templated by breath figures，Polymer Chemistry，201405，5，17，5175-5182，SCI，IF=5.520，他引2次。

[7] 朱凉伟、杨武、欧洋、万灵书*、徐志康，Synthesis of polystyrene with cyclic, ionized and neutralized end groups and the self-assemblies templated by breath figures，Polymer Chemistry，

201404，5，11，3666-3672，SCI，IF=5.520，他引3次。

[8]　朱凉伟、吴柏衡、万灵书*、徐志康，Polystyrene with hydrophobic end groups: Synthesis, kinetics, interfacial activity, and self-assemblies templated by breath figures，Polymer Chemistry，201402，5，14，4311-4320，SCI，IF=5.520，他引2次。

[9]　吴柏衡、朱凉伟、欧洋、汤文、万灵书*、徐志康，Systematic investigation on the formation of honeycomb-patterned porous films from amphiphilic block copolymers，Journal of Physical Chemistry C，201501，119，4，1971-1979，SCI，IF=4.772，他引1次。

[10]　欧洋、王黎阳、朱凉伟、万灵书*、徐志康，In-situ immobilization of silver nanoparticles on self-assembled honeycomb-patterned films enables surface-enhanced Raman scattering (SERS) substrates，Journal of Physical Chemistry C，201405，118，21，11478-11484，SCI，IF=4.772，他引8次。

[11]　欧洋、朱凉伟、肖文达、杨皓程、江庆军、李霞、吕建国、万灵书*、徐志康，Nonlithographic fabrication of nanostructured micropatterns via breath figures and solution growth，Journal of Physical Chemistry C，201402，118，8，4403-4409，SCI，IF=4.772，他引6次。

[12]　朱凉伟、万灵书*、金晶、徐志康，Honeycomb porous films prepared from porphyrin-cored star polymers: Submicrometer pores induced by transition of monolayer into multilayer structures，Journal of Physical Chemistry C，201303，117，12，6185-6194，SCI，IF=4.772，他引10次。

[13]　陈鹏程、万灵书*、柯蓓蓓、徐志康，Honeycomb-patterned film segregated with phenylboronic acid for glucose sensing，Langmuir，201109，27，20，12597–12605，SCI，IF=4.457，他引30次。

[14]　柯蓓蓓、万灵书*、陈鹏程、章路遥、徐志康，Tunable assembly of nanoparticles on patterned porous film，Langmuir，201010，26，20，15982-15988，SCI，IF=4.457，他引18次。

[15]　万灵书*、柯蓓蓓、张菁、徐志康，Pore shape of honeycomb-patterned films: Modulation and interfacial behavior，Journal of Physical Chemistry B，201201，116，1，40-47，SCI，IF=3.302，他引17次。

出版著作教材共0本，总字数为0万字，其中为主编、副主编出版全国统编教材0本，省部重点、规划教材共0本：（不超过10本）

(填写格式：所有作者姓名，书名，著作类型，出版地，出版社名称，出版年月，个人字数/总字数)

3.3 承担或参与的主要科研、教改项目

1、共参加项目12项，其中纵向项目11项，横向项目1项；
主持项目到校总经费452.1万元，其中纵向项目到校经费252.1万元，横向项目到校经费200万元。

2、作为项目负责人承担项目11项，其中纵向项目10项，横向项目1项。具体项目如下(请按您认为最具代表性、重要性或影响力的顺序列出)：(不超过15项)

(填写格式：项目名称，项目性质及来源，项目编号，项目经费（括号内为本人实际承担经费，单位万元），起始年月，终止年月，项目成员）)

[1]　高分子分离膜的表面与界面，纵向，国家自然科学基金优秀青年科学基金项目，51522305，150万(已到款0万)，2016-01-01，2018-12-31，万灵书。

[2]　有序多孔膜表面的浸润性转变及其调控研究，纵向，国家自然科学基金委员会，21374100，82万(已到款65.6万)，2014-01-01，2017-12-31，万灵书。

[3]　孔径单分散高分子分离膜的制备及结构调控研究，纵向，国家自然科学基金委员会，51173161，60万(已到款60万)，2012-01-01，2015-12-31，万灵书。

[4]　糖基化蜂窝状有序膜的制备及其集束效应研究，纵向，国家自然科学基金委员会，50803053，20万(已到款20万)，2009-01-01，2011-12-31，万灵书。

[5] 基于界面共形沉积的复合均孔膜的制备与应用研究，纵向，浙江省公益性技术应用研究计划项目，2015C31028，15万(已到款15万)，2015-01-01，2016-12-31，万灵书。

[6] 基于多层次自组装的有序多孔膜定点功能化研究，纵向，浙江省自然科学基金会，Y4110076，10万(已到款10万)，2011-01-01，2012-12-31，万灵书。

[7] 塑料基纤维膜表面物理结构调控及性能研究，高性能塑料及其先进加工技术，纵向，浙江省重点创新团队自主设计一般项目，2009R50004-13，13万(已到款13万)，2010-09-01，2013-08-31，万灵书。

[8] 多孔纳米纤维吸附材料，横向，企业，112301-I21401/005，200万(已到款200万)，2014-01-01，2017-12-31，万灵书。

[9] 高分子均孔膜制备的基底研究，纵向，中央高校基本科研业务费优秀青年人才计划，112301*172210352，50万(已到款50万)，2015-08-01，2016-12-31，万灵书。

[10] 高分子膜材料的可控制备与功能化，纵向，中央高校基本科研业务费青年专项资助计划，2014QNA4037，12.5万(已到款12.5万)，2014-01-01，2015-12-31，万灵书。

[11] 孔径单分散高分子微孔膜制备与结构控制研究，纵向，中央高校基本科研业务费科研基地发展专项，2011KYJD010，6万(已到款6万)，2011-01-01，2011-12-31，万灵书。

[12] 高分子化学实验课程的交互式教学研究，浙江省2013年高等教育课堂教学改革项目，kg2013017，排名5/5。

3.4 获得的重要成果奖励

共获成果奖4项，其中教材奖0项，教学成果奖0项，科研成果奖4项，国家发明专利0项，请按您认为最具代表性、重要性或影响力的顺序列出：(不超过10项)

(填写格式：项目名称，奖励名称，奖励级别，授奖单位，获奖年月，本人排名/总人数)

[1] 基于高性能膜分离材料的水处理技术集成与应用，宁波市科学技术奖，一等奖，宁波市人民政府，201403，10/13。

[2] 静电纺纳米纤维膜表面固定化过氧化氢酶研究，浙江省自然科学学术奖，三等奖，浙江省自然科学学术奖评审委员会，201211，1/4。

[3] Honeycomb-patterned film segregated with phenylboronic acid for glucose sensing，“十一五”浙江省自然科学基金优秀论文，浙江省自然科学基金委员会，201209，1/4。

[4] 静电纺纤维膜的制备、表面修饰与酶固定化研究，浙江省高等学校科研成果奖，一等，浙江省教育厅，201012，1/5。

3.5 任国际期刊编委、国际学术会议重要职务及在国际学术会议全会报告、特邀报告情况

[1] SCI期刊Int. J. Polym. Sci.客座编辑

[2] Ling-Shu Wan, Preparation of Isoporous Membranes for Cell Separation. The 9th Conference of Aseanian Membrane Society (AMS9), July 19-21, 2015, Taipei, Oral talk.

[3] Ling-Shu Wan, Perforated Isoporous Membranes for High-Resolution and Low-Fouling Separation of Cells at Low Operation Pressure. 5th China-Europe Symposium on Biomaterials in Regenerative Medicine, April 7-10, 2015, Hangzhou, China, Oral talk.

[4] Ling-Shu Wan, Directed self-assembly of ternary blends of block copolymer and homopolymers on chemical patterns, The 57th International Conference on Electron, Ion, and Photon Beam Technology & Nanofabrication, May 28-31, 2013, Nashville, USA, Oral talk.

[5] Ling-Shu Wan, Application of Cassie-Wenzel Transition on Functionalization of Self-organized Honeycomb-patterned Porous Films. The 2nd Federation of Asian Polymer Societies (FAPS) Polymer Congress, May 8-11, 2011, Beijing, China, Oral talk.

3.6 获得专利情况

共获专利18项，其中发明专利18项。请按您认为最具代表性、重要性或影响力的顺序列出：（不超过10项）

(填写格式：专利名称，专利类型，专利授权国，专利号，授权公告年月，本人排名/总人数)

[1] 基于呼吸图有序多孔膜的表面增强拉曼散射基底的制备方法，发明专利，中国，ZL201310304368.2，201504，1/5
[2] 一种自支撑贯通型聚电解质有序多孔膜的制备方法，发明专利，中国，ZL201310035447.8，201407，1/5
[3] 用于葡萄糖检测的有序多孔膜的制备方法及其应用，发明专利，中国，ZL201110020592.X，201207，1/5
[4] 一种有机无机复合蜂窝状有序膜的制备方法，发明专利，中国，ZL201110020587.9，201205，1/5
[5] 分子识别分离膜及其制备方法与应用，发明专利，中国，ZL201010262050.9，201202，1/3
[6] 由固定化脂肪酶－透水膜生物反应器制备生物柴油的方法，发明专利，中国，ZL200810060314.5，201109,1/3
[7] 一种用于油脂水解的固定化脂肪酶的制备方法，发明专利，中国，ZL200910097896.9，201102，1/4
[8] 一种抗菌聚合物分离膜的制备方法，发明专利，中国，ZL201010256455.1，201208，2/3
[9] 由固定化脂肪酶－多孔膜生物反应器制备生物柴油的方法，发明专利，中国，ZL 200810060549.4，201111，2/3
[10] 由固定化脂肪酶－透醇膜生物反应器制备生物柴油的方法，发明专利，中国，ZL200810060548.X，201105，2/3

3.7 其他获奖及荣誉称号

[1] 2013年浙江大学求是青年学者
[2] 2012年浙江大学高分子系“聚合先锋”优秀共产党员
[3] 2011-2012学年秋冬学期浙江大学求是学院蓝田学园优秀班主任
[4] 2011年浙江大学叶萍奖教金

3.8 社会服务及兼职等

[1] 积极参加浙江省新型吸附分离材料与应用技术重点实验室、吸附分离材料联合实验室的建设工作
[2] 国家自然科学基金评审专家、浙江省自然科学基金评审专家
[3] 国际知名期刊Chem. Soc. Rev., J. Am. Chem. Soc., Adv. Mater., Adv. Func. Mater., ACS Nano, Sci. Rep.等三十余种期刊的审稿人
[4] 新生之友：2014级、2015级
[5] 2014年09月－至今：蓝田材化1406班主任
[6] 2011年09月－2012年06月：蓝田1135班主任
[7] 指导本科生国家级大学生创新创业训练计划项目2项5人次、浙江省大学生科技创新计划项目7项13人次、指导SRTP4项10人次。

四、 申请人主要学术成绩、贡献、创新点及其科学价值或社会经济意义(不超过3000字)

聚合物分离膜是面向能源、资源、环境和医疗等国家重大需求的高新材料。目前，相转化法制备的超微滤膜应用最为广泛。具有可控表面性质的孔径单分散膜被广泛认为是下一代高性能分离膜的发展方向。申请人围绕具有可控表面性质的孔径单分散分离膜这一目标，潜心聚合物多孔膜及其表界面基础研究，取得了以下创新性成果：[1] 首创基于呼吸图法的孔径单分散聚合物分离膜材料的制备，建立了此类膜材料的多层次结构调控方法，进而实现了细胞等物质在超低压条件下的精密分离；[2] 拓展和完善了孔径单分散膜材料制备的界面理论，发现了膜表面浸润性转变规律，提出了以区域选择性为特征的界面功能化新策略。近五年以通讯作者在J. Am. Chem. Soc.等期刊发表 SCI 论文 27 篇，其中 IF > 4 论文 21 篇，SCI 他引 239 次；获国家发明专利授权 18 项；应邀在 Chem. Commun.撰写综述论文；以第一完成人获浙江省高校科研成果一等奖等学术奖励。

学术贡献一：具有精密分离功能的孔径单分散聚合物膜及其多层次结构调控

呼吸图法是制备孔径单分散多孔膜材料最为简单有效的方法之一，且与目前已工业化应用的相转化法具有兼容的制备流程，在材料科学领域引起了广泛的关注。我们发现以冰面作为成膜基底可同时解决界面铺展性和成膜稳定性这两个关键问题，从而首次实现了贯通孔膜的可控制备。进一步推广至甘油等有机溶剂表面，发现较大的铸膜液/基底界面张力和适当曲率的变形可能是贯通孔形成的重要原因，并首次对其形成机理进行了定量描述。提出了一种基于冰面的无转移法制备孔径单分散膜的新策略，获得了可灭菌的干态膜，实现了无外加压力下对酵母和乳酸菌的高效分离，对酵母的截留率接近 100%、乳酸菌的回收率超过 70%且活性得到保持，所制备的孔径单分散膜表现出良好的应用前景。(J. Am. Chem. Soc. 2012, 134, 95; Chem. Commun. 2014, 50, 4024; ACS Appl. Mater. Interfaces 2014, 6, 22400; J. Phys. Chem. C 2014, 118, 4403; J. Phys. Chem. C 2015, 119, 1971)

进一步建立了孔径单分散膜的单层/多层结构、孔径、孔道形态等多层次结构的调控方法。大尺度调控膜的孔径是一直受到重视但没有得到有效解决的关键问题之一。发现聚合物结构的微小变化可以极其显著地影响所制备膜的形态。以四臂星形聚合物为例，与苯乙烯均聚物膜相比，引入仅 2 个单体单元的亲水“嵌段”后所形成的膜具有截然不同的形态：从单层孔结构转变为多层孔结构，膜孔孔径则从微米级别显著降低至 100 – 500 纳米。另一方面，通过调控溶剂与亲水性添加剂的相互作用，阐明了界面张力对孔道形态的影响规律，实现了孔道在球形、椭球形和 U 形之间的可控转变，这是为数不多的能有效调控膜孔孔道形态的途径。(J. Phys. Chem. B 2012, 116, 40; J. Phys. Chem. C 2013, 117, 6185; J. Phys. Chem. B 2014, 118, 845; Polym. Chem. 2014, 5, 3666; Polym. Chem. 2014, 5, 4311; Polym. Chem. 2014, 5, 5175)

上述具有精密分离功能的孔径单分散聚合物膜材料及其多层次结构调控研究成果的科学价值表现在：发展了一种新颖的孔径单分散分离膜材料的制备方法，实现了无外加压力条件下的精密分离，对拓展聚合物多孔膜材料科学内涵与研发下一代高性能分离膜材料具有重要意义；对贯通孔形成机制的阐述不但有利于促进对呼吸图法制备孔径单分散多孔膜机理的全面理解，还为发展普适性的成膜基底提供了基础；基于聚合物结构及其界面行为的研究则为膜结构形态调控提供了丰富而有效的手段。

这些工作得到了国内外同行的广泛关注、评价和跟踪研究：

① 基于申请人在聚合物多孔膜材料及其表界面研究领域的创新性成果和系统性工作，被邀请在 Chem. Commun. (2014, 50, 4024)发表题为“Multiple Interfaces in Self-assembled Breath Figures”的专题论文。该论文短时间内被 Angew. Chem.等期刊论文他引 22 次。

② 发表于 J. Am. Chem. Soc. (2012, 134, 95) 的研究论文被 J. Am. Chem. Soc.和 Angew. Chem.等期刊论文他引 53 次。例如，澳大利亚技术科学与工程院院士、J. Membr. Sci.前编辑 Fane 教授以图表形式引用了我们的结果，并评价为制备孔径单分散聚合物分离膜的代表性方法之一(ACS Nano 2013, 7, 1882)；西班牙聚合物技术研究所的 Rodriguez- Hernandez 教授在 Prog. Polym. Sci. (2014, 39, 510)一文中引用了我们的多项工作，并作了正面的详细评论，认为我们实现了高精度分离，所采用的冰面成膜方法易于转移。

③ 值得指出的是，上述工作发表后得到国内外多个课题组的跟踪研究，采用我们提出的冰面成膜法制备了不同聚合物材料的孔径单分散膜，并进行了类似的精密分离实验 (例如：Soft Matter 2012, 8, 8835; Macromol. Rapid Commun. 2014, 35, 221)。这不但表明我们的工作引起了同行的关注和兴趣，也证明我们所提出的方法对不同成膜聚合物具有较好的普适性。

学术贡献二：孔径单分散膜表面浸润性转变规律与区域选择性界面功能化策略

聚合物分离膜的表面(包括孔壁)被认为与其本体多孔特性具有几乎同等的重要性，这是因为膜表面性质对其服役稳定性特别是抗污染能力具有重要影响，而且在亲和/智能分离过程中扮演重要角色。申请人系统研究了水溶性聚合物、亲水嵌段、亲水基团和微凝胶等不同体系的界面富集与组装行为，发现亲水组分显著富集于铸膜液/水滴界面，进而保留在膜孔孔壁。例如，富集在膜孔孔壁的苯硼酸基团显著促进了对葡萄糖的检测灵敏度；以界面富集的活性羟基作为平台，通过表面引发可控接枝聚合等策略构筑了糖阵列，系统研究了糖与蛋白质的相互作用，为蛋白质亲和检测与分离膜材料的可控制备提供了基础；进一步将基团的界面自组装拓展到酶等生物大分子，提出并实现了一步构建辣根过氧化物酶图案化功能膜的新方法。(Langmuir 2011, 27, 12597; Soft Matter 2011, 7, 4221; Chem. Commun. 2012, 48, 4417)

聚合物多孔膜表面的浸润性现象及其规律对构建刺激响应性表面和粘附表面具有重要意义。通过监测孔径单分散膜在层层自组装过程中的表面亲水性和平均膜厚度，首次发现了此类膜材料表面的 Cassie – Wenzel 浸润性转变现象，阐明了表面浸润性的变化规律及其原因。尤其值得指出的是，上述表面浸润性变化规律的认识为膜孔的功能化提供了崭新的思路：利用这一独特的浸润性转变现象，通过巧妙设计实验实现了纳米颗粒和微球在膜表面的区域选择性组装。与膜表面浸润性转变类似，发现通过多巴胺沉积与后功能化等手段可以有效调控水滴在膜表面的粘附。 (Langmuir 2010, 26, 15982; ACS Appl. Mater. Interfaces 2010, 2, 3759; Phys. Chem. Chem. Phys. 2011, 13, 4881; Chem. Commun. 2013, 49, 10522; J. Phys. Chem. C 2014, 118, 11478; J. Phys. Chem. C 2015, 119, 3667)

上述孔径单分散膜表面浸润性转变与区域选择性功能化策略研究成果的科学价值表现在：对孔径单分散聚合物膜材料形成过程中界面现象的创新与系统研究揭示了水滴界面所起到的重要角色及其最终塑造膜孔结构与表面化学的规律，为原位制备区域选择性功能化多孔膜材料提供了理论基础和技术途径；有关孔径单分散膜材料表面浸润性转变的理论发现和应用的系列工作不但显著促进了对此类膜材料的界面物理化学的深入理解，还建立了调控膜表面浸润性和粘附力及其转变的新策略，对具有可控表面性质孔径单分散膜材料的制备具有重要意义。

国内外同行对上述工作给予了重视：

① 利用浸润性转变来实现区域选择性功能化的工作不但得到同行的引用和评价，也给予同行一定的启发。例如，西班牙 de Leon 等人在其发表于 Polym. Chem. (2013, 4, 4024)的研究论文中，以单独一段 200 余单词的篇幅详细介绍了我们报道的浸润性转变现象及膜表面区域选择性功能化策略，指出我们实现了膜孔、膜孔外以及全部表面的选择性修饰，并强调了我们选择性修饰膜孔的方法，进而此为基础报道了基于点击化学的膜孔外的选择性修饰。

② 申请人的工作还得到了国内外大部分同行的重视。例如，以界面富集的羟基为平台的工作，他引 43 次，唐本忠院士、澳大利亚 Davis 教授和 Stenzel 教授、西班牙 Rodriguez-Hernandez 教授和 Munoz-Bonilla 教授等人都作了正面引用和评述，被认为是界面功能化的代表性工作之一。

③ 有关膜表面浸润性转变的工作被 Phys. Chem. Chem. Phys. (2011, 13, 4881)期刊的“基于界面物理与化学的材料创新”专辑收录，发表后得到 Adv. Mater. (2011, 23: 5817)等期刊论文的引用。

五、其他能反映学术研究水平的突出业绩

申请人以通讯作者于 2009 年和 2010 年发表的 3 篇 SCI 论文共被他引 251 次，其中单篇最高他引 178 次。

[1] Zhen-Gang Wang, **Ling-Shu Wan***, Xiao-Jun Huang, Zhen-Mei Liu, Zhi-Kang Xu*. Enzyme immobilization on electrospun polymer nanofibers: An overview. ***Journal of Molecular Catalysis-B Enzymatic*** 2009, 56: 189-195. *(Most Cited Journal of Molecular Catalysis B: Enzymatic Articles since 2007, 201205; Most Downloaded Journal of Molecular Catalysis B: Enzymatic Articles, 201205)* **他引 178 次**

[2] Bei-Bei Ke, **Ling-Shu Wan***, Zhi-Kang Xu. Controllable construction of carbohydrate microarrays by site-directed grafting on self-organized porous films. ***Langmuir*** 2010, 26(11): 8946-8952. **他引 43 次**

[3] Bei-Bei Ke, **Ling-Shu Wan***, Wen-Xu Zhang, Zhi-Kang Xu. Controlled synthesis of linear and comb-like glycopolymers for honeycomb-patterned films. ***Polymer*** 2010, 51(10): 2168-2176. **他引 30 次**

个人承诺

本人保证：所从事的学术研究符合学术道德规范要求；所提供的材料客观真实。

承诺人： 万灵书

2015年10月20日

上述材料均已审核，内容真实，与证明材料原件相符。

审核人：

年　　　月　　　日

JACS
JOURNAL OF THE AMERICAN CHEMICAL SOCIETY
Communication
pubs.acs.org/JACS

Ordered Microporous Membranes Templated by Breath Figures for Size-Selective Separation

Ling-Shu Wan,* Jun-Wei Li, Bei-Bei Ke, and Zhi-Kang Xu

MOE Key Laboratory of Macromolecular Synthesis and Functionalization, Department of Polymer Science and Engineering, Zhejiang University, Hangzhou 310027, China

Ⓢ *Supporting Information*

ABSTRACT: Membranes with highly uniform pore size are important in various fields. Here we report the preparation and performance of ordered membranes, the pore diameter of which is on the micrometer scale. The ordered membranes fabricated at two-phase interfaces enable a high-resolution and energy-saving separation process. Moreover, a possible mechanism for the formation of through-pores has been proposed and experimentally verified.

Porous membranes are important not only in industrial applications but also in some advanced fields such as microfluidics, biosensing, and catalysis.[1−7] Microporous membranes are often employed to remove impurities or byproducts through size-selective filtration for sample pretreatment or post-treatment. For example, the sample can be that for chromatography or light scattering measurements. It is well known that the pore size and its distribution are crucial to the size-selective separation performance of the membranes. They are therefore strongly desired to have pores with narrow size distribution and ordered structures, as such membranes possess extra separation accuracy, require only low or ultralow operation pressure, and show some interesting features such as significantly enhanced mass transport rates.[8−11]

The track etch method was adapted to fabricate membranes with highly uniform pore size, but this method is limited to polycarbonate and poly(ethylene terephthalate), and the pore density is low. Self-assembly of block copolymers has attracted much attention over the past decades. Bicontinuous or cylindrical microphase separated domains can be formed in the assembled film by varying preparation conditions such as annealing and by modulating the balance of repulsive interactions between dissimilar segments of the copolymers. The domains may be selectively removed, leaving well-ordered pore channels.[8−16] Recently, the block copolymers have been advanced from polystyrene-*block*-poly(ethylene oxide)[14] to polyethylene-based copolymers;[15] the self-assembly process was combined with non-solvent-induced phase separation to fabricate asymmetric membranes.[16] It is generally believed that microphase separation of block copolymers leads to domains in the range of 10−100 nm.[17,18] In this Communication, we describe a method to prepare ordered membranes with highly uniform pore size on the micrometer scale for size-selective separation. The ordered membranes enable a high-resolution and energy-saving separation process.

An amphiphilic block copolymer, polystyrene-*block*-poly(*N*,*N*-dimethylaminoethyl methacrylate) (PS-*b*-PDMAEMA), that was synthesized by atom-transfer radical polymerization,[19,20] was used to prepare ordered membranes. The copolymer was dissolved in carbon disulfide (CS_2), and 100 μL of the as-prepared solution was cast at a two-phase interface under a humid airflow. The relative humidity was controlled above 70%. During this process, condensed water droplets arrange into ordered arrays, i.e., the so-called breath figures, and act as dynamic templates for the pores.[21,22] It has been reported that properties of the interfaces (e.g., air/solid and air/water interfaces) have a great impact on the pore structures.[23−27] For example, the air/glass interface often leads to dead-end pores which may be considered as picoliter beakers[28] or microreactors.[29] Formation of through-pores is a prerequisite for preparation of ordered separation membranes. In this work, the block copolymer solution was cast at an air/ice interface. Figure 1 shows SEM micrographs of the typical ordered membrane with hexagonal pore arrays. As can be seen from the micrographs of the top, bottom, and cross section of the

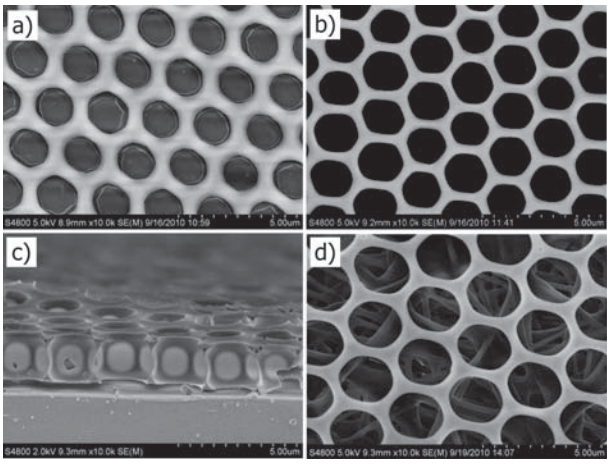

Figure 1. SEM images of the typical ordered membrane with through-pores, prepared from 1 mg/mL of PS-*b*-PDMAEMA solution in CS_2 at an air/ice interface. The airflow speed is 4 L/min. (a) Top, (b) bottom, and (c) cross section. (d) The membrane transferred onto a piece of dense nanofiber mesh.

Received: October 2, 2011
Published: December 5, 2011

membrane, the pores are of through structure. The membrane was further transferred onto a piece of dense electrospun nanofiber mesh.[30] Nanofibers below the ordered membrane can be clearly observed through the pores. Moreover, the pore diameter of the membranes can be facilely modulated in the range of 1−5 μm by changing the solution concentration and airflow speed (Figure S1, Supporting Information (SI)).

The thickness of the ordered membrane is about 2 μm (Figure 1c). It is not free-standing but can be easily transferred onto various supports such as silicon, gold, and porous meshes. Therefore, we fabricated composite membranes using a stainless steel woven wire mesh as the support (Figure 2). A composite membrane with ordered separation layer has been achieved (Figure 2d). As marked by the arrow in Figure 2b, a thin layer of polystyrene nanofibers was deposited on the mesh surface to enhance both the integrity of the ordered membrane and the interfacial adhesion between the membrane and the mesh.[30] The sparse nanofiber layer has irregular and large pores of tens of micrometers without affecting the separation performance of the composite membrane. Figure 2f shows photographs of the composite membrane and a permeation module. This module is a commercially available one that is often used for sample pretreatment such as in dynamic light scattering measurements.

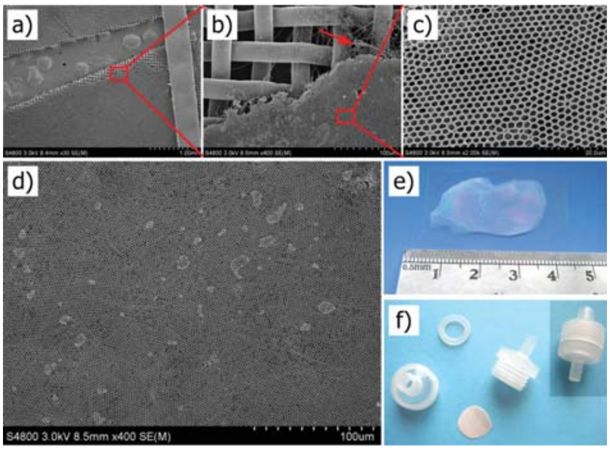

Figure 2. (a−d) SEM images of the composite membrane with different magnifications. (e) Digital photograph of a piece of ordered membrane. (f) Digital photographs of the composite membrane and the membrane module used for separation.

Figure 3 shows the size distribution of polystyrene particles before and after filtration by the composite membrane, the separation layer of which has a pore diameter of 3 μm. The feed microspheres have a bimodal size distribution peaking at 2.0 and 5.0 μm. Interestingly, the filtrates show a single peak, and the curve is accurately cut off at about 3 μm; that is, the ordered membrane shows high-resolution separation performance. Moreover, it should be mentioned that the separation can be carried out without additional pressure. As we know, traditional microfiltration processes generally need 0.1 MPa or higher additional pressure, depending on pore sizes (also the three-dimensional structure) and properties of the membrane material. Therefore, it can be concluded that this ordered membrane enables a high-resolution and energy-saving separation process.

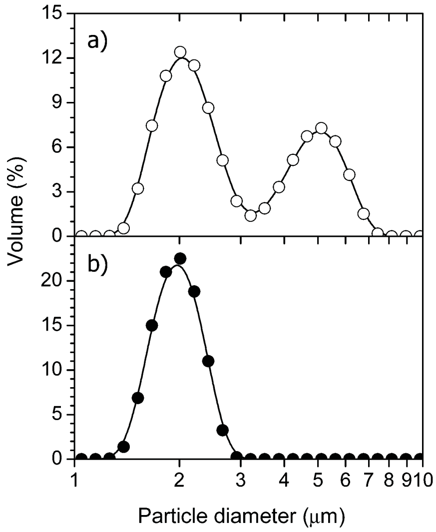

Figure 3. (a) Size distribution of the feed polystyrene microspheres with bimodal distribution at 2.0 and 5.0 μm. (b) Size distribution of the microspheres after filtration by a composite membrane, the pore diameter of which is 3 μm.

We tried some other block copolymers, including polystyrene-*block*-poly(2-hydroxyethyl methacrylate) (PS-*b*-PHEMA)[31] and polystyrene-*block*-poly(acrylic acid) (PS-*b*-PAA),[32] and compared their membrane-forming properties at the air/ice and air/water interfaces (Figure S2, SI). We found that the polymer solution spreads better at the air/ice interface than at the air/water interface. The spreading leads to larger membrane areas with hexagonal arrays of monodisperse through-pores instead of dead-end pores. By contrast, the cast solution on water surface tends to form ellipsoid and hence provides longer time to grow for water droplets condensed in the thicker center area. After complete evaporation of water and the organic solvent, pores at the membrane center are larger than those at the edge area. Apart from the spreading behavior, low temperature may be another reason for the regular structure at the air/ice interface. It has been reported that evaporation of the solvent rapidly cools the solution, which is important to the formation of regular arrays of water droplets because the cooling induces a temperature gradient.[33] Our results show that water with lower temperature leads to higher regularity (Figure S3, SI). Therefore, the membrane with through-pores is more regular when prepared at the air/ice interface than at the air/water interface. This finding makes it possible to prepare ordered membranes from some commonly used polymers.

The pore structure may be affected by the vertical position of water droplets in the polymer solution at the moment of membrane hardening (Figure 4a). Besides the thermocapillary and Marangoni forces,[33] the density of the solvent can affect the position of water droplets. When benzene is used as the solvent for the polymer solution, through-pore structures are obtained with smaller round pores on the top and larger ones on the bottom.[23] Chloroform solutions, by contrast, generate pores with larger diameter on the top and smaller diameter on the bottom.[27] What we envisage is that low-density benzene ($\rho = 0.87$ g mL^{-1}) allows the condensed water droplets ($\rho = 1.00$ g mL^{-1}) to submerge into the bottom of the polymer solution, leading to larger pore size on the bottom, while in the case of

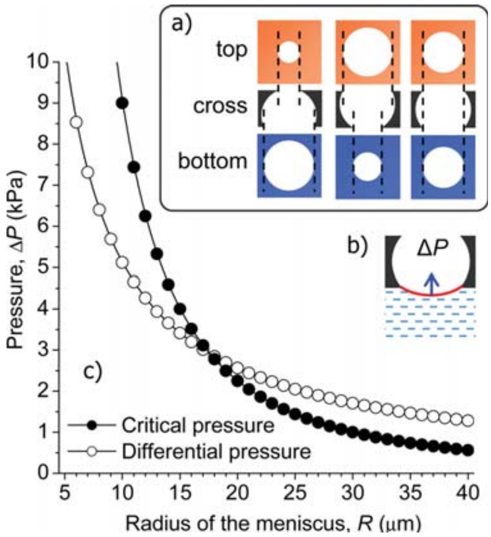

Figure 4. (a) Pore structures of ordered membranes prepared from solutions using benzene, chloroform, and CS_2 (from left to right) as the solvent. (b) Illustration of the formation of through-pores. (c) Calculated curves of differential pressure and critical differential pressure vs the radius according to eqs 1 and 2.

chloroform (ρ = 1.48 g mL^{-1}) the pores are the opposite of those found in the benzene system. In the present work, the density of CS_2 (ρ = 1.26 g mL^{-1}) is between those of benzene and chloroform, and hence, the through-pores show almost the same diameter on the top and the bottom.

It is clear that the density of the solvent can influence the pore structure, which implies water droplets are falling in the polymer solution during the film formation. The through-pore structure is proposed to be induced by fusion of water droplets in the polymer solution with the substrate, i.e., thin water layer on the ice surface or bulk water in our case.[23,27] However, how the pores become through-pores is still unclear. There should be a very thin film between the water droplets and the substrate because phase inversion takes place when polymer solution and non-solvent meet.[34] Such thin films can be sometimes observed in films cast from solutions with high polymer concentration (Figure S4, SI). Differing from hard substrate, soft substrate such as water allows further falling of the water droplets, which leads to the deformation of the thin film and induces meniscuses toward the substrate (Figure 4b). With the evaporation of the water droplets, there is a differential pressure, ΔP, induced by the surface tension of the substrate liquid across the meniscus, and the relationship is given as[35]

$$\Delta P = \frac{2\gamma}{R} \tag{1}$$

where γ is the interfacial tension of the substrate/thin film (liquid/solid) interface, and R is the radius of the meniscus. Interfacial tension of polystyrene/water is about 25.6 mN m^{-1},[36] and R is always larger than the radius of the pore diameter. The curve of ΔP vs R can therefore be plotted according to eq 1. However, for an ultrathin polymer film it is very difficult to measure or accurately calculate the critical differential pressure, ΔP_c, at which the film ruptures. Through-pores can be formed only when ΔP is larger than ΔP_c. It has been reported that for a polymer hollow microsphere with a wall thickness of δ, ΔP_c is expressed as[37,38]

$$\Delta P_c = \frac{4E}{3}\left(\frac{\delta}{R}\right)^2 \tag{2}$$

where E is Young's modulus of the polymer. The Young's modulus of dry polystyrene is about 3000 MPa, which slightly changes with the molecular weight and temperature[39] and drastically decreases with the presence of solvent. The thickness of the thin film, which is generated by phase inversion as mentioned above, is estimated from SEM images to be about 15 nm (Figure 1c). Therefore, a curve of ΔP_c vs R can be obtained according to eq 2. As can be seen from the two calculated curves (Figure 4c), ΔP induced by the interfacial tension exceeds ΔP_c of the film when $R > 18$ μm. In other words, the possible thin film can be easily broken by the differential pressure, forming through-pores. It should be noted that the values of film thickness, interfacial tension, and the Young's modulus do not change the trends of ΔP and ΔP_c.

Based on the above-mentioned mechanism, other liquids that provide enough interfacial tension may theoretically be considered as substrates for the preparation of ordered membranes with through-pores. Membranes prepared on the surface of glycerol and formic acid support our hypothesis (Figure S5, SI). However, through-pore membranes cannot be fabricated on the surface of acetic acid, tetraethyl orthosilicate, ethyl acetate, ethanol, isopropanol, and methanol, which are of low surface tension and low density. Experimentally, the cast solution was observed sinking into the soft substrates with low density. Besides, our preliminary results show that an ordered membrane with through-pores can be prepared from a commercially available polymer, polystyrene, although the membrane-forming window is very narrow (Figure S6, SI). The use of other substrates and commercial available polymers not only extends the application range of the ordered membranes but also increases the easy availability of this method.

In summary, this Communication reports ordered microporous membranes with highly uniform pore size. The membranes were prepared at the interface of air/ice, which can be extended to the interfaces of air/glycerol and air/formic acid. A static model has been proposed for the calculation of critical pressure for rupture of the thin film and the applied pressure. If the applied pressure exceeds the critical pressure, the formation of through-pores becomes possible. We demonstrated the capability of the corresponding composite membranes for high-preciseness separation of polystyrene microspheres with close sizes. The membranes only require ultralow operation pressure, enabling an energy-saving separation process.

■ ASSOCIATED CONTENT

Ⓢ Supporting Information

Experimental details and effects of substrates. This material is available free of charge via the Internet at http://pubs.acs.org.

■ AUTHOR INFORMATION

Corresponding Author

lswan@zju.edu.cn

■ ACKNOWLEDGMENTS

This work was supported by the National Natural Science Foundation of China (51173161, 50803053), and partially supported by the Zhejiang Provincial Natural Science

Foundation of China (Y4110076), the Program for Zhejiang Provincial Innovative Research Team (2009R50004), and the Open Fund of Zhejiang Provincial Top Key Discipline of New Materials and Process Engineering (20110932). J.-W.L. thanks the Zhejiang Provincial Undergraduate Scientific and Technological Innovation Project (2011R401163) for support.

REFERENCES

(1) Ulbricht, M. *Polymer* **2006**, *47*, 2217.

(2) de Jong, J.; Lammertink, R. G. H.; Wessling, M. *Lab Chip* **2006**, *6*, 1125.

(3) Baker, L. A.; Choi, Y. S.; Martin, C. R. *Curr. Nanosci.* **2006**, *2*, 243.

(4) Weder, C. *Angew. Chem., Int. Ed.* **2008**, *47*, 448.

(5) Shannon, M. A.; Bohn, P. W.; Elimelech, M.; Georgiadis, J. G.; Marinas, B. J.; Mayes, A. M. *Nature* **2008**, *452*, 301.

(6) Wan, L. S.; Liu, Z. M.; Xu, Z. K. *Soft Matter* **2009**, *5*, 1775.

(7) Huang, J. X.; Pradel, K. C.; Sohn, K. *Angew. Chem., Int. Ed.* **2011**, *50*, 3412.

(8) Wei, Q. H.; Bechinger, C.; Leiderer, P. *Science* **2000**, *287*, 625.

(9) Kim, J. K.; Yang, S. Y.; Ryu, I.; Kim, H. Y.; Jang, S. K.; Russell, T. P. *Adv. Mater.* **2006**, *18*, 709.

(10) Yang, S. Y.; Park, J.; Yoon, J.; Ree, M.; Jang, S. K.; Kim, J. K. *Adv. Funct. Mater.* **2008**, *18*, 1371.

(11) Yang, S. Y.; Yang, J. A.; Kim, E. S.; Jeon, G.; Oh, E. J.; Choi, K. Y.; Hahn, S. K.; Kim, J. K. *ACS Nano* **2010**, *4*, 3817.

(12) Chen, L.; Phillip, W. A.; Cussler, E. L.; Hillmyer, M. A. *J. Am. Chem. Soc.* **2007**, *129*, 13786.

(13) Li, X. F.; Fustin, C. A.; Lefevre, N.; Gohy, J. F.; De Feyter, S.; De Baerdemaeker, J.; Egger, W.; Vankelecom, I. F. J. *J. Mater. Chem.* **2010**, *20*, 4333.

(14) Kim, S. H.; Misner, M. J.; Xu, T.; Kimura, M.; Russell, T. P. *Adv. Mater.* **2004**, *16*, 226.

(15) Pitet, L. M.; Amendt, M. A.; Hillmyer, M. A. *J. Am. Chem. Soc.* **2010**, *132*, 8230.

(16) Peinemann, K. V.; Abetz, V.; Simon, P. F. W. *Nat. Mater.* **2007**, *6*, 992.

(17) Bernards, D. A.; Desai, T. A. *Soft Matter* **2010**, *6*, 1621.

(18) Wang, Y.; Li, F. B. *Adv. Mater.* **2011**, *23*, 2134.

(19) Ke, B. B.; Wan, L. S.; Chen, P. C.; Zhang, L. Y.; Xu, Z. K. *Langmuir* **2010**, *26*, 15982.

(20) Wan, L. S.; Lv, J.; Ke, B. B.; Xu, Z. K. *ACS Appl. Mater. Interfaces* **2010**, *2*, 3759.

(21) Widawski, G.; Rawiso, M.; Francois, B. *Nature* **1994**, *369*, 387.

(22) Srinivasarao, M.; Collings, D.; Philips, A.; Patel, S. *Science* **2001**, *292*, 79.

(23) Nishikawa, T.; Ookura, R.; Nishida, J.; Arai, K.; Hayashi, J.; Kurono, N.; Sawadaishi, T.; Hara, M.; Shimomura, M. *Langmuir* **2002**, *18*, 5734.

(24) Bunz, U. H. F. *Adv. Mater.* **2006**, *18*, 973.

(25) Stenzel, M. H.; Barner-Kowollik, C.; Davis, T. P. *J. Polym. Sci., Part A: Polym. Chem.* **2006**, *44*, 2363.

(26) Gugliuzza, A.; Aceto, M. C.; Macedonio, F.; Drioli, E. *J. Phys. Chem. B* **2008**, *112*, 10483.

(27) Ma, H. M.; Cui, J. W.; Song, A. X.; Hao, J. C. *Chem. Commun.* **2011**, *47*, 1154.

(28) Erdogan, B.; Song, L. L.; Wilson, J. N.; Park, J. O.; Srinivasarao, M.; Bunz, U. H. F. *J. Am. Chem. Soc.* **2004**, *126*, 3678.

(29) Li, X.; L., X. F.; Zhang, L. A.; Wang, Y. X.; Yang, X. L.; Zhao, N.; Zhang, X. L.; Xu, J. *J. Am. Chem. Soc.* **2011**, *133*, 3736.

(30) Wan, L. S.; Ke, B. B.; Wu, J.; Xu, Z. K. *J. Phys. Chem. C* **2007**, *111*, 14091.

(31) Ke, B. B.; Wan, L. S.; Xu, Z. K. *Langmuir* **2010**, *26*, 8946.

(32) Chen, P. C.; Wan, L. S.; Ke, B. B.; Xu, Z. K. *Langmuir* **2011**, *27*, 12597.

(33) Maruyama, N.; Koito, T.; Nishida, J.; Sawadaishi, T.; Cieren, X.; Ijiro, K.; Karthaus, O.; Shimomura, M. *Thin Solid Films* **1998**, *327*, 854.

(34) Guillen, G. R.; Pan, Y. J.; Li, M. H.; Hoek, E. M. V. *Ind. Eng. Chem. Res.* **2011**, *50*, 3798.

(35) Youngblood, J. P.; McCarthy, T. J. *Macromolecules* **1999**, *32*, 6800.

(36) Absolom, D. R.; Neumann, A. W. *Colloids Surf.* **1988**, *30*, 25.

(37) Gao, C. Y.; Leporatti, S.; Moya, S.; Donath, E.; Mohwald, H. *Langmuir* **2001**, *17*, 3491.

(38) Gao, C. Y.; Donath, E.; Moya, S.; Dudnik, V.; Mohwald, H. *Eur. Phys. J. E* **2001**, *5*, 21.

(39) Ellis, B.; Smith, R., *Polymers: A Property Database*, 2nd ed.; CRC Press: Boca Raton, FL, 2009.

ChemComm

Dynamic Article Links

Cite this: *Chem. Commun.*, 2012, **48**, 4417–4419

www.rsc.org/chemcomm

COMMUNICATION

Patterned biocatalytic films *via* one-step self-assembly†

Ling-Shu Wan,* Qing-Lian Li, Peng-Cheng Chen and Zhi-Kang Xu

Received 29th November 2011, Accepted 11th January 2012
DOI: 10.1039/c2cc17451k

Patterned porous films containing enzymes have been facilely prepared *via* a one-step breath figure process, which is based on the self-assembly of horseradish peroxidase nanoparticles that show good resistance to organic solvents. The patterned biohybrid films possess robust catalytic activity.

Patterned films containing biomolecules show great potential applications in various fields including biology, biosensing, biomedical technology, and tissue engineering.[1] For example, patterns of enzymes are useful in high-throughput screening of chemical libraries.[2] Horseradish peroxidase (HRP) is an enzyme that catalyzes the oxidation of numerous phenols and aromatic amines as well as many other reactions. It has been widely used as a component of clinical diagnostic kits and for immunoassays.[3] The most common pathway to fabricate patterned biohybrid films is top-down techniques such as lithography.[4] Although these techniques are commercially viable, they suffer from high equipment costs and require additional procedures for the attachment of biomolecules.[4] As an alternative to the top-down techniques, bottom-up approaches have received considerable attention, which generally employ self-assembly processes.[5] However, they also involve multiple steps in most cases, and it is difficult to immobilize biomolecules to specific regions of the patterned films. Therefore, one-step formation of patterned biohybrid films is still a big challenge so far.

The breath figure method, inspired by the foggy arrays of water droplets on cool surfaces, is a versatile, convenient, and cost-saving bottom-up technique for fabricating patterned porous films.[6–9] The self-assembly of hydrophilic groups and nanoparticles (NPs) induces hierarchically ordered structures during the film formation, providing the possibility of one-step formation of patterned biohybrid films.[9–11] However, the breath figure method often uses organic solvents with high saturation vapour pressure such as chloroform and carbon disulfide, in which most biomolecules, especially enzymes, are unstable or poorly soluble.

In this communication, we describe a one-step method to fabricate patterned films containing HRP. The films were prepared *via* the breath figure method by casting polymer solution dispersed with HRP NPs, which are composed of a HRP core and a hydrophilic cross-linked polymer shell. The polymer shell protects the HRP against organic solvents. During the film formation, the NPs stabilized the condensed water droplets and spontaneously formed patterns.

HRP NPs were synthesized according to the literature.[12] Vinyl HRP was polymerized at 25 °C using acrylamide as monomer, *N*,*N*′-methylene bisacrylamide as cross-linker, and 4-dimethylaminoantipyrine as stabilizer (Fig. 1). FT-IR spectra confirm the introduction of vinyl groups and the polymer shell (Fig. S1 and S2, ESI†). We prepared HRP400 and HRP800 NPs with monomer/HRP molar ratios of 400 and 800, respectively. TEM images show that free HRP, HRP400 NPs, and HRP800 NPs have average diameters of 8.9, 14.8, and 20.3 nm, respectively. Dynamic light scattering measurements provide similar results (Fig. S3, ESI†). The polydispersity indices (PDI) are 0.171, 0.166, and 0.139, respectively. The size of free HRP is consistent with that reported in the literature.[12] The relatively large PDI may be due to the aggregation of HRP. The HRP400 NPs are spherical and the diameter is

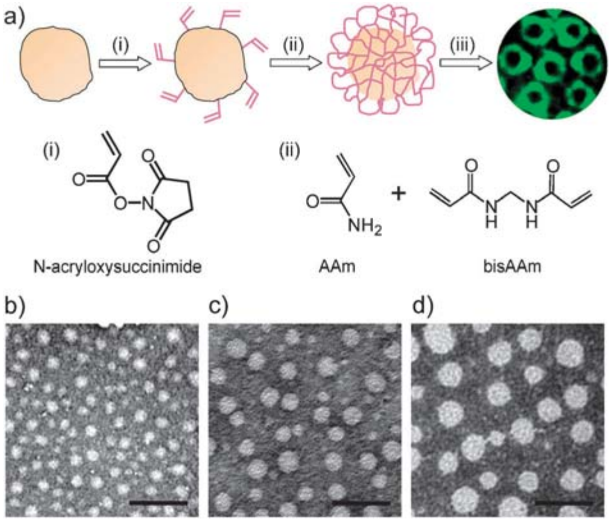

Fig. 1 (a) Synthesis of HRP NPs and preparation of HRP patterns. (i) Vinyl groups were introduced to the HRP molecule surface. (ii) AAm and bisAAm were copolymerized on vinyl HRP to form a thin cross-linked shell. (iii) HRP NPs were added to polystyrene/chloroform solution to form patterned films *via* the breath figure method. (b–d) TEM images of (b) free HRP, (c) HRP400 NPs, (d) HRP800 NPs. Scale bar: 50 nm.

MOE Key Laboratory of Macromolecular Synthesis and Functionalization, Department of Polymer Science and Engineering, Zhejiang University, Hangzhou 310027, China.
E-mail: lswan@zju.edu.cn; Fax: +86 571 87951592;
Tel: +86 571 87953763

† Electronic supplementary information (ESI) available: Synthesis, characterization and activity assay of the HRP NPs; preparation and characterization of the HRP patterns. See DOI: 10.1039/c2cc17451k

doubled compared to free HRP. Moreover, FT-IR spectra confirm the existence of a large amount of polymer around HRP (Fig. S2, ESI†). Therefore, we conclude that most HRP NPs only contain one HRP molecule. It should be noted that HRP400 NPs were used in this work because the size is closer to that of free HRP than HRP800 NPs. In the following text, HRP NPs means HRP400 NPs unless otherwise specified.

HRP NPs dispersed in ethanol were added to chloroform solution of polystyrene (PS), and then the mixtures were cast under a humid environment to form patterned porous films. Fig. 2 shows typical SEM images of the films. More SEM images are shown in Fig. S4 (ESI†). A small amount of HRP NP dispersion can remarkably improve the regularity of the films. Films prepared from mixtures containing 1–7 vol% HRP NP dispersion show hexagonal pore arrays, whereas those prepared from PS or mixtures with more than 8 vol% HRP NP dispersion are not very ordered. The added HRP NP dispersion also has a great influence on the pore diameter (Fig. 2c) and the pore shape (Fig. S5, ESI†) of the films.

It is generally accepted that in the breath figure method, condensed water droplets get close to the three-phase line and hexagonally arrange under the thermocapillary and Marangoni forces.[7,13] The water droplets can be stabilized by the precipitated polymer or adsorbed NPs at the interface and hence do not fuse. The formed pores are shaped by the stabilized water droplets, the shape of which depends on the spreading behavior on the solution surface. The spreading coefficient S is defined as follows:[14]

$$S = \gamma_{sg} - (\gamma_{wg} + \gamma_{ws}) \tag{1}$$

where γ_{sg} is the surface tension of the polymer solution, γ_{wg} is the surface tension of the water droplet, and γ_{ws} is the interfacial tension between the polymer solution and the water droplet in this case (Fig. 2d). The adsorption of NPs at the interface of water/oil can remarkably decrease the interfacial tension, γ_{ws},[15] leading to the increase of spreading coefficient. As a result, the water droplets become flatter compared with those in a PS/chloroform system. Obviously, flatter water droplets lead to flatter pores and hence larger pore diameters. On the other hand, with further increasing the amount of NPs, the size of droplets stabilized by the NPs decreases[16] and the pore diameters decrease accordingly. Therefore, the pore diameters of the films increase first and then decrease with the amount of HRP NP dispersion.

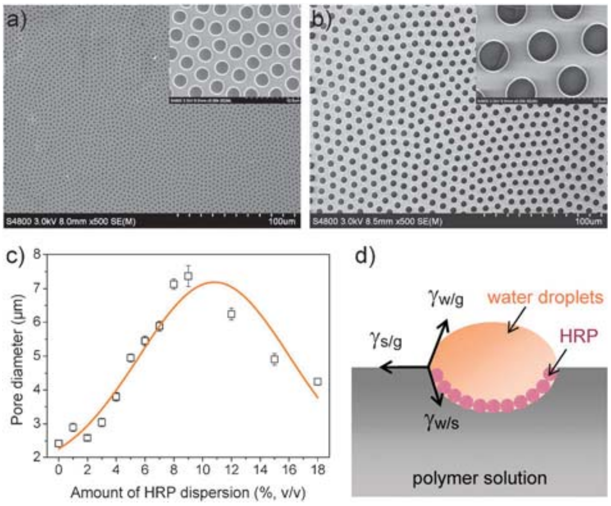

Fig. 2 (a,b) SEM images of patterned porous films prepared from (a) PS and (b) PS solution containing 6 vol% HRP NPs. PS concentration is 30 mg mL^{-1}. Scale bar: 100 µm (inset: scale bar is 10 µm). (c) Dependence of pore diameter of the films on the amount of HRP NPs added to the cast solution (0–18 vol%). (d) Illustration of water droplets stabilized by HRP NPs during the formation of breath figures.

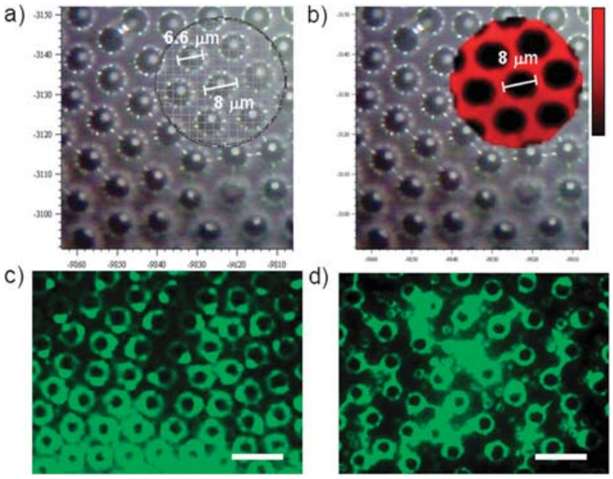

Fig. 3 (a) Optical image of patterned porous film containing HRP NPs with a pore diameter of ~6.6 µm. (b) Confocal Raman spectroscopy image at a Raman shift of 1003 cm^{-1}, which was stacked on the corresponding optical image. The scattering intensity increases with color changing from black to red. (c,d) Confocal laser scanning microscopy images of films with FITC-labeled (c) HRP NPs and (d) free HRP. Scale bar: 20 µm.

If the water droplets are indeed stabilized by HRP NPs, the pore walls will be decorated with HRP NPs. It has been reported that hard NPs such as CdSe and SiO_2 NPs can assemble at the pore walls.[10,11] Here, we demonstrate that the pore walls were decorated with soft NPs such as free HRP or HRP NPs. Fig. 3 shows high-resolution confocal Raman spectroscopy and confocal laser scanning microscopy (CLSM) images of the patterned porous films containing HRP. The Raman shift at 1003 cm^{-1} corresponds to a typical peak for PS (Fig. S6, ESI†).[17] A Raman image was recorded at this Raman shift in a circular region with a diameter of 32 µm. It can be seen that the Raman image exhibits an excellent pattern, where the red area denotes high concentration of PS whereas the black area suggests poor signal of PS. The poor signal can be caused by both low concentration of PS and difficulty in collecting the scattering signal. The black area corresponding to the pore bottom may be attributed to the difficulty in collecting the scattering signal. However, the "pore" diameter determined from the Raman image is about 8 µm, which is obviously larger than the actual diameter of the pore measured from the corresponding optical image (~6.6 µm). The black transition area corresponds to the pore walls with a thickness of about 0.7 µm. In this ring area the poor signal of PS may be induced by its low concentration because of the segregation of HRP NPs. Moreover, in the pore area the Raman shift at 1618 cm^{-1} caused by HRP[18] is stronger than those of PS although the scattering signal of HRP NPs is relatively weak

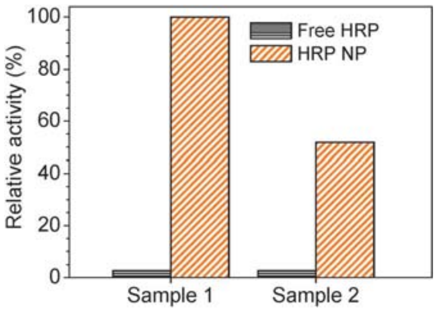

Fig. 4 Relative activity of films patterned with free HRP and HRP NPs. Sample 1: films prepared from as-dispersed free HRP or HRP NPs in ethanol; Sample 2: films stored for 7 days at 4 °C.

(Fig. S6, ESI†). The patterns can also be clearly observed from the CLSM images of film samples cast from solutions containing FITC-labeled HRP NPs (Fig. 3c and Fig. S7, ESI†). For comparison, FITC-labeled free HRP was used for film preparation. Patterned porous film with segregated HRP was also obtained (Fig. 3d). Therefore, it seems that a large amount of HRPs segregated at the pore walls.

Next, we measured the activity and stability of free HRP and HRP NPs in solutions according to the procedure proposed by Nicell and Wright.[19] In the activity assays, we must use the same amount of HRP. To this end, the absorption intensity of HRP NPs at 403 nm, where the extinction coefficient is 102 mM^{-1} cm^{-1}, was kept the same as that of free HRP. At the optimal reaction temperature for free HRP, HRP NPs possess more than 90% residual activity ($\sim$510 units) when compared with free HRP ($\sim$560 units) (Fig. S8, ESI†). Results also indicate that HRP NPs possess better thermal stability. To evaluate the resistance to organic solvents, the activity of HRP NPs was measured in aqueous solutions containing 15% methanol, 15% tetrahydrofuran, or up to 80% ethanol (Fig. S8, ESI†). Obviously, HRP NPs show better activity than free HRP in the mixtures containing organic solvents. As for other organic solvents such as chloroform and carbon disulfide that are often used in the breath figure method, it is difficult to measure the activity of HRPs because these organic solvents are immiscible with water.

Fig. 4 shows the activity and stability of HRP in the patterned porous films. The film prepared from as-dispersed HRP in ethanol completely loses the activity (sample 1), let alone that stored for 7 days at 4 °C (sample 2). The film prepared from HRP NPs, by contrast, retains obvious activity; furthermore, the residual activity reaches 52% after stored for 7 days at 4 °C. It should be noted that Fig. 4 gives the normalized data because we did not know the exact amount of HRP that participates in the reaction. Part of the HRP may be embedded in the film and cannot participate in the reaction.

The hydrophilic cross-linked polymer shell around HRP has a thickness of only several nanometres (Fig. 1) and hence shows little influence on the diffusion of the substrates to the active site of HRP.[12] Therefore, the HRP NPs still show very high residual activity. On the other hand, their good resistance to organic solvents may be ascribed to the improved structural integrity *via* multipoint linkage, the increased intramolecular hydrogen bonds, and the retained essential water of enzyme by the hydrophilic shell.[20] Therefore, the HRP NPs can be dispersed in organic solvents for one-step preparation of patterned biocatalytic films.

In summary, we have demonstrated a one-step approach to the fabrication of patterned porous films containing horseradish peroxidase (HRP). The films were prepared from polystyrene solutions dispersed with HRP NPs *via* the breath figure method. The HRP dispersion shows great influence on the regularity, pore diameter, and pore shape of the patterned films. During the process of film formation, HRP NPs stabilized the condensed water droplets and formed HRP patterns with obvious catalytic activity, which were confirmed by high-resolution confocal Raman spectroscopy and confocal laser scanning microscopy. This approach opens a facile route to one-step fabrication of patterned biocatalytic films.

This work was supported by the NNSFC (51173083, 50803053), and partially supported by the ZJNSFC (Y4110076) and Fundamental Research Funds for the Central Universities (MOE Engineering Research Center of Membrane and Water Treatment Technology). The authors thank Dr Qiaoshi Zeng in Zhejiang University for helping with confocal Raman spectroscopy measurements.

Notes and references

1 D. B. Weibel, W. R. DiLuzio and G. M. Whitesides, *Nat. Rev. Microbiol.*, 2007, **5**, 209–218.
2 D. P. Funeriu, J. Eppinger, L. Denizot, M. Miyake and J. Miyake, *Nat. Biotechnol.*, 2005, **23**, 622–627.
3 O. Ryan, M. R. Smyth and C. O. Fagain, *Essays Biochem.*, 1994, **28**, 129–146.
4 G. M. Whitesides, E. Ostuni, S. Takayama, X. Y. Jiang and D. E. Ingber, *Annu. Rev. Biomed. Eng.*, 2001, **3**, 335–373.
5 (*a*) S. H. Kim, M. J. Misner, T. Xu, M. Kimura and T. P. Russell, *Adv. Mater.*, 2004, **16**, 226–231; (*b*) Y. Zhang and C. Wang, *Adv. Mater.*, 2007, **19**, 913–916; (*c*) E. H. Min, K. H. Wong and M. H. Stenzel, *Adv. Mater.*, 2008, **20**, 3550–3556.
6 G. Widawski, M. Rawiso and B. Francois, *Nature*, 1994, **369**, 387–389.
7 (*a*) M. Srinivasarao, D. Collings, A. Philips and S. Patel, *Science*, 2001, **292**, 79–83; (*b*) U. H. F. Bunz, *Adv. Mater.*, 2006, **18**, 973–989; (*c*) M. H. Stenzel, C. Barner-Kowollik and T. P. Davis, *J. Polym. Sci., Part A: Polym. Chem.*, 2006, **44**, 2363–2375.
8 (*a*) B. B. Ke, L. S. Wan, P. C. Chen, L. Y. Zhang and Z. K. Xu, *Langmuir*, 2010, **26**, 15982–15988; (*b*) B. B. Ke, L. S. Wan, Y. Li, M. Y. Xu and Z. K. Xu, *Phys. Chem. Chem. Phys.*, 2011, **13**, 4881–4887; (*c*) P. C. Chen, L. S. Wan, B. B. Ke and Z. K. Xu, *Langmuir*, 2011, **27**, 12597–12605.
9 B. B. Ke, L. S. Wan and Z. K. Xu, *Langmuir*, 2010, **26**, 8946–8952.
10 A. Boker, Y. Lin, K. Chiapperini, R. Horowitz, M. Thompson, V. Carreon, T. Xu, C. Abetz, H. Skaff, A. D. Dinsmore, T. Emrick and T. P. Russell, *Nat. Mater.*, 2004, **3**, 302–306.
11 W. Sun, J. Ji and J. C. Shen, *Langmuir*, 2008, **24**, 11338–11341.
12 M. Yan, J. Ge, Z. Liu and P. K. Ouyang, *J. Am. Chem. Soc.*, 2006, **128**, 11008–11009.
13 M. F. Schatz and G. P. Neitzel, *Annu. Rev. Fluid Mech.*, 2001, **33**, 93–127.
14 H. Dobbs and D. Bonn, *Langmuir*, 2001, **17**, 4674–4676.
15 Z. W. Niu, J. B. He, T. P. Russell and Q. Wang, *Angew. Chem., Int. Ed.*, 2010, **49**, 10052–10066.
16 B. P. Binks, J. Philip and J. A. Rodrigues, *Langmuir*, 2005, **21**, 3296–3302.
17 P. Musto, A. Borriello, P. Agoretti, T. Napolitano, G. Di Florio and G. Mensitieri, *Eur. Polym. J.*, 2010, **46**, 1004–1015.
18 S. Z. Hu, K. M. Smith and T. G. Spiro, *J. Am. Chem. Soc.*, 1996, **118**, 12638–12646.
19 J. A. Nicell and H. Wright, *Enzyme Microb. Technol.*, 1997, **21**, 302–310.
20 (*a*) W. Piyatheerawong, Y. Iwasaki, X. B. Xu and T. Yamane, *J. Mol. Catal. B: Enzym.*, 2004, **28**, 19–24; (*b*) J. Ge, D. N. Lu, J. Wang, M. Yan, Y. F. Lu and Z. Liu, *J. Phys. Chem. B*, 2008, **112**, 14319–14324.

ACS APPLIED MATERIALS & INTERFACES
Research Article
www.acsami.org

Fabrication of Perforated Isoporous Membranes via a Transfer-Free Strategy: Enabling High-Resolution Separation of Cells

Yang Ou,[†] Chang-Jiang Lv,[‡] Wei Yu,[†] Zheng-Wei Mao,[†] Ling-Shu Wan,*,[†] and Zhi-Kang Xu[†]

[†]MOE Key Laboratory of Macromolecular Synthesis and Functionalization, Department of Polymer Science and Engineering, and [‡]State Key Laboratory of Chemical Engineering, Department of Chemical and Biochemical Engineering, Zhejiang University, Hangzhou 310027, People's Republic of China

Supporting Information

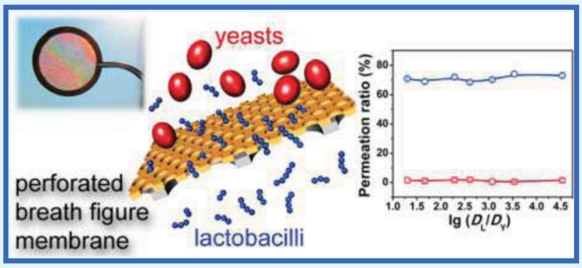

ABSTRACT: Thin perforated membranes with ordered pores are ideal barriers for high-resolution and high-efficiency selective transport and separation of biological species. However, for self-assembled thin membranes with a thickness less than several micrometers, an additional step of transferring the membranes onto porous supports is generally required. In this article, we present a facile transfer-free strategy for fabrication of robust perforated composite membranes via the breath figure process, and for the first time, demonstrate the application of the membranes in high-resolution cell separation of yeasts and lactobacilli without external pressure, achieving almost 100% rejection of yeasts and more than 70% recovery of lactobacilli with excellent viability. The avoidance of the transfer step simplifies the fabrication procedure of composite membranes and greatly improves the membrane homogeneity. Moreover, the introduction of an elastic triblock copolymer increases the interfacial strength between the membrane and the support, and allows the preservation of composite membranes in a dry state. Such perforated ordered membranes can also be applied in other size-based separation systems, enabling new opportunities in bioseparation and biosensors.

KEYWORDS: *porous materials, isoporous membranes, self-assembly, breath figures, cell separation*

1. INTRODUCTION

Cell separation is important in environmental protection, healthcare, food, and biotechnology industries, for example, yeast harvesting in beer brewing,[1] specific capture and detection of circulating tumor cells in blood,[2−5] and isolation of stem, blood, and tissue cells.[6−10] Separation of eukaryotic cells (e.g., yeasts) from prokaryotic cells (e.g., lactobacilli) is essential for the diagnosis of bacterial infections and food contaminations.[11,12] Typically, yeasts play a substantial role in the spoilage of commercial fruit yogurts fermented by lactobacillus bacteria.[11] Currently, a series of cell separation techniques have been developed,[13] among which centrifugation and membrane filtration are the most commonly used techniques. As cell separation through centrifugation is a time-consuming and labor-intensive process, membrane filtration provides a rapid, simple, energy-saving, and inexpensive method and has been widely applied to large-scale bioseparation including cell separation.[14,15] However, commonly used membranes prepared by phase inversion exhibit a high pore coefficient of variation (CV > 20%) and large thickness (typically several tens of micrometers) with tortuous pore paths, resulting in a low separation accuracy and huge flow resistance.[16] Alternatively, perforated membranes with ordered pore arrays are ideal for high-resolution and efficient biological transport and separation.[17−20]

Up to now, techniques for fabricating perforated membranes include track etching, anodization, lithographic microfabrication, and self-assembly approaches such as colloidal crystal assembly, emulsion templating, breath figures, and microphase separation of block copolymers.[16,21−24] Although track etched and anodized aluminum oxide membranes with micrometer-sized ordered pores have been commercially available, the former still suffers from low pore density (~15%) and the later is costly. Furthermore, both of the commercialized membranes have long pore channels (~15−20 μm), which are promising in single file diffusion[16−20,25] but require relatively high operation pressure. It should be noted that high operation pressure is not desirable for cell separation because of the possible viability loss of cells which are sensitive to physical stresses, and besides, high operation pressure may induce unexpected cell permeation through membranes with a pore size much smaller than the cell size because of cell deformation. Self-assembly processes offer a promising alternative to fabricate ultrathin perforated membranes, which enable not only an extra separation accuracy but also a low or ultralow operation pressure and a significant enhancement of mass transport rates.[23] For example, in a previous communication we reported an ordered membrane

Received: September 18, 2014
Accepted: November 25, 2014
Published: November 25, 2014

dx.doi.org/10.1021/am506419z | *ACS Appl. Mater. Interfaces* 2014, 6, 22400−22407

prepared at an ice/air interface followed by a transfer step, which shows perfect size-selective separation of polystyrene microspheres.[26] Although Peinemann et al. has reported an integral (nontransfer) preparation of asymmetric membranes by the combination of nonsolvent-induced phase separation and self-assembly of amphiphilic block copolymers,[27−32] for self-assembled thin perforated membranes with a thickness less than several micrometers, an additional step of transferring the membranes onto porous supports is generally required.[33−36] Because of the high porosity of perforated structures and the inherent fragility of membrane materials, pore cracks may occur in the transfer process, which attenuates the separation selectivity and mechanical durability of the membranes. In addition, it is important to strengthen the interfacial adhesion between membranes and the supports so that it will be feasible to recover cells or reduce membrane fouling by back flushing. Moreover, most self-assembled membranes and even some phase inversion membranes that have a thickness of several tens of micrometers must be preserved in wet state (e.g., in glycerin) to prevent from possible pore collapse during the drying process. For cell separation, membranes need to be sterilized before use, and thus membranes that can be preserved at a dry state are highly desirable.

Here we present a facile transfer-free strategy for fabrication of robust perforated composite membranes via a self-assembly process and the application in cell separation. The transfer step is avoided in this method, which simplifies the procedure of fabricating composite membranes and greatly improves the homogeneity of the membranes; on the other hand, blending an elastic triblock copolymer further increases the interfacial adhesion strength between the membrane and the porous support. As a result of the rational design of the fabrication process as well as membrane-forming material chemistry, the composite membranes are able to be preserved in dry state and durable to back flushing. Separation of mixtures of yeasts and lactobacilli demonstrated almost 100% rejection of yeasts and more than 70% recovery of lactobacilli. The permeated lactobacilli show excellent viability, which is confirmed by cell culture experiments. We believe that this is the first example of cell separation using a thin perforated self-assembled membrane without external pressure, which can also be applied in other size-based separation systems, enabling new opportunities in bioseparation and biosensors. Moreover, the proposed transfer-free strategy provides a new pathway to prepare other composite materials.

2. EXPERIMENTAL SECTION

Materials. The synthesis of polystyrene-*block*-poly(*N*,*N*-dimethylaminoethyl methacrylate) (PS_{247}-*b*-$PDMAEMA_{14}$, M_n = 27 900 g mol^{-1}, M_w/M_n = 1.24) by atom transfer radical polymerization was described elsewhere.[37] Polystyrene-*block*-polyisoprene-*block*-polystyrene (SIS, 22 wt % styrene, M_n = 158600 g mol^{-1}, M_w/M_n = 1.18) was purchased from Sigma-Aldrich and used as received. Transmission electron microscopy (TEM) grids (Φ12 mm) were purchased from Beijing Xinxing Braim Technology Co. Ltd. (China) and used as porous supports. Before used, the TEM grids were sonicated with acetone for 15 min and blow-dried by nitrogen gas. Poly(ethylene terephthalate) (PET) films were kindly provided by Hangzhou Tape Factory (China) and cleaned with acetone for 5 min and repeated three times before used. The yeast strains, *Saccharomyces cerevisiae* (*S. cerevisiae*), were purchased from Zhejiang Microbiology Institute (China). The lactobacillus strains, *Streptococcus thermophilus* (*S. thermophilus*), were purchased from China Center of Industrial Culture Collection. Water used in the experiments was deionized and ultrafiltrated to 18.2 MΩ with an ELGA LabWater system. All other reagents were acquired from Sinopharm Chemical Reagent Co. Ltd. (China) and used without further purification.

Transfer-Free Fabrication Method. Perforated honeycomb composite membranes were prepared at an air/ice interface according to the following procedure.[26] Typically, a cleaned TEM grid was placed in a PS Petri dish (Φ 30 mm) and covered by a thin ice layer with a thickness of ∼1 mm. Then, a solution of PS_{247}-*b*-$PDMAEMA_{14}$/SIS (40 μL) in carbon disulfide (CS_2) was drop-cast onto the surface of ice well above the TEM grid under a humid airflow at room temperature. The concentration of PS_{247}-*b*-$PDMAEMA_{14}$ was fixed at 1 mg mL^{-1} while the SIS weight fraction in the blends varied from 0 to 80 wt %. The relative humidity of the airflow, measured by a hygrothermograph (DT-321S, CEM Corporation), was maintained around 80% by bubbling through distilled water, and the flow rate was controlled via a needle valve and measured by a flow meter. A thin turbid solution film formed on the ice/water surface in merely several seconds. As the evaporation of CS_2 and condensed water droplets, the thin ice layer above the TEM grid gradually melted into water and infiltrated down through the wide openings of the grid, which leads to self-adhesion of the honeycomb membrane onto the TEM grid. Consequently, a composite membrane was directly fabricated without further membrane transfer steps in only several minutes. To prevent the honeycomb membrane from unexpected cracking induced by the capillary force during water evaporation, we immersed the as-prepared composite membrane in ethanol for 10 s to completely replace the water remaining in the pores before drying in the air at room temperature. The composite membranes in the dry state could be stored well with no obvious cracks for more than 30 days.

Membrane Characterizations. The integrity and interfacial adhesion strength of the honeycomb membranes were assessed by microscope images obtained from an optical microscopy (Ti−U, Nikon). The integrity ratio, *I*, is defined as the ratio of TEM grid area covered by honeycomb membranes with none-cracking pores (S_H) to the whole TEM grid dimension (S_T), which is given as

$$I = \frac{S_H}{S_T} \times 100\%$$

The average integrity ratio is obtained from 5 parallel pieces of composite membranes and the integrity of each membrane is calculated from 3 random locations.

The assessment of interfacial adhesion strength is borrowed from the method for evaluating paint adhesion force. Perforated honeycomb membranes transferred on PET films were prepared and pressed by an adhesive Scotch tape onto the membrane surface. The adhesion ratio, *A*, is defined as the ratio of residual area of membranes after the unfirm pore structures were peeled off from the support (S_R) to the whole PET film dimension (S_P), which is given as

$$A = \frac{S_R}{S_P} \times 100\%$$

The average adhesion ratio is obtained from 5 parallel pieces of honeycomb membranes on PET films and the adhesion strength of each membrane is calculated from 3 random locations.

The pore diameter distribution of the honeycomb membranes was statistically analyzed by measuring the pore sizes of over 100 pores on the top and bottom surface through the corresponding SEM images, respectively.

Cell Separation Assay. A honeycomb composite membrane with a diameter of 12 mm was mounted in a homemade permeation module. Before filtration, the composite membrane was sterilized in 75% alcohol for 10 min and rinsed by physiological saline three times to completely replace the air captured in the pores and wet the membrane surface. Yeasts and lactobacilli were mixed and dispersed in physiological saline with various cell densities. The separation was performed in a dead-end mode without any additional pressure. The feed cell dispersion was flowed through the filter chamber and the filtrate was collected in a 10 mL vial for subsequent characterization. The cell separation process was recorded by a real-time monitoring optical video (see the Supporting Information, Movie S1: yeast filtration, the yeast cell density in the feed solution is 3.4×10^6 cfu mL^{-1}; Movie S2: separation of mixtures of yeasts and lactobacilli, the cell density of yeasts and lactobacilli in the feed solution was 3.4×10^6 and 6.8×10^7 cfu mL^{-1}, respectively). On the other hand, the sterilization and rinsing process were the same for the sucking filtration method. The feed solution of yeast cells in a vial was sucked up into the syringe at a speed of about 0.25 mL min^{-1}. The permeation ratio of a specific type of cells is defined as the proportion of the cell density in the filtrate solution to that in the feed.

The cell density of yeasts and lactobacilli was obtained by cell counting via a hemocytometer and from OD600 values by an UV−vis spectrophotometer (UV-2450, Shimadzu), respectively. The relationship between the cell density and OD600 values of yeasts was determined by the results of cell counting and UV adsorption value, giving the yeast cell density of 1.46×10^7 cfu mL^{-1} at OD600 = 1.0. The relationship between the cell density and OD600 values of lactobacilli was established according to the National food safety standard food microbiological examination (GB 4789.35−2010), which shows the lactobacillus cell density of 3.89×10^8 cfu mL^{-1} at OD600 = 1.0.

3. RESULTS AND DISCUSSION

Transfer-Free Membrane Fabrication. Inspired by water droplet arrays condensed on cold substrates, the breath figure technique provides a simple, robust, and efficient strategy to fabricate honeycomb membranes with a pore size range of submicrometer to tens of microns.[38−47] As pioneered by Parisi and co-workers,[48] honeycomb membranes with perforated pore structures were successfully prepared via depositing a dilute polymer solution on liquid surface with an adequately large surface tension (e.g., water).[26,49−55] We originally demonstrated the use of ice as the substrate for preparing perforated honeycomb membranes.[26] Traditionally, a polymer solution is cast onto water or ice surface with a dimension and thickness far beyond that of the resultant honeycomb membrane,[26,49−55] and the as-prepared membrane will be finally floating on water surface. Then, the membrane can be carefully transferred to supports. In theory, only the outermost surface layer of the substrate (e.g., water) is essential to the formation of perforated membranes.[26] Obviously, a membrane would spontaneously adhere to the support on a lowering water surface.[56] Hence, it is possible to prepare perforated honeycomb membranes on a thin ice layer without further transfer steps. Typically, porous supports, such as TEM grids, were placed in a PS Petri dish (Φ 30 mm) and covered by a thin ice layer with a thickness of ∼1 mm (Figure 1a). A solution of PS-*b*-PDMAEMA/SIS blends in CS_2 was drop-cast onto the air/ice interface well above the TEM grid under a humid airflow with ∼80% relative humidity (Figure 1b). The polymer solution would spread at the air/ice interface, resulting in a thin, disk-like, turbid solution film on the ice/water surface in merely several seconds. The diameter of the solution film was about 17 mm, which is slightly larger than that of a TEM grid. Condensed water droplets induced by evaporative cooling self-assemble into hexagonal arrays as a result of Marangoni convection and thermocapillary force, and penetrate the polymer solution film induced by the excess of the surface tension differential pressure to the critical rupture pressure across the pores (Figure 1c).[26] As the evaporation of CS_2 and water, the thin ice layer above the TEM grid gradually melts into water and infiltrates down through the wide openings of the grid, leading to self-adhesion of the membrane onto the underlying TEM grid (Figure 1d). Consequently, a composite membrane can be directly fabricated without membrane transfer steps in only several minutes (Figure 1e).

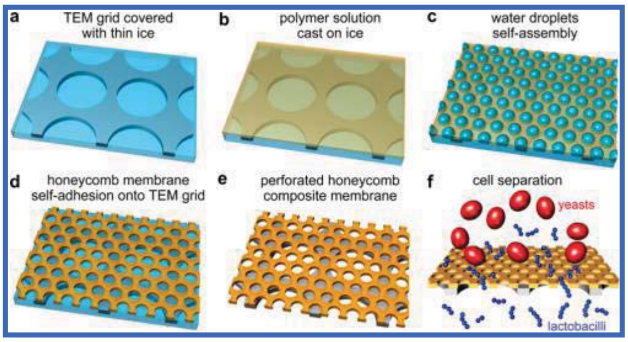

Figure 1. Schematic illustrations of the fabrication of perforated honeycomb membranes on porous supports such as TEM grids via (a−e) a transfer-free breath figure method and (f) the cell separation process.

A typical perforated honeycomb composite membrane is shown in Figure 2a−f. By using PS-*b*-PDMAEMA/SIS (60 wt % SIS) blends as the membrane-forming material, perforated honeycomb membranes without pore cracks in a large area were obtained via the transfer-free method. Typically, the membrane has a pore diameter of 2.5 μm on the top surface (Figure 2a, b) and 2.7 μm at the bottom (Figure 2c, d). It is noteworthy that, compared to other self-assembled membranes, the pore size of the perforated honeycomb membranes is in the micrometer range, which is well-suited for cell separation. Meanwhile, the membrane presents a considerably high porosity of up to 70% within a single opening of the TEM grid support, and a thin membrane thickness of about 2 μm (Figure 2e and Supporting Information, Figure S1e). Besides the TEM grid, other porous supports such as stainless steel sieves, nylon fabrics, and nanofibrous meshes can also be used. Moreover, it should be emphasized that we prepared highly uniform honeycomb membranes with a remarkably low pore CV down to 3.85% on both the top and bottom surface (Figure 2g). The composite membrane displays uniform bright iridescent colors when viewed with a reflected light (Figure 2f), indicating the formation of a perfectly ordered honeycomb composite filter with a membrane diameter of 12 mm (more than 1.1 cm^2, inset of Figure 2f). Generally, the maximum membrane area could be up to several square centimeters, which depends on the volume of the casting solution and the scale of supports. The high homogeneity, perfectly perforated structure, high porosity, and thin thickness may endow the membrane with high-resolution separation ability at ultralow operation pressure.

Compared to other fabrication techniques for perforated polymeric membranes with ordered pores, such as track etching, photolithography, colloidal crystal templating, and microphase separation of block copolymers, this transfer-free breath figure method allows the formation of relatively large-area membranes in a simple and time-saving way. Besides, water is utilized as templates in this method, which is nontoxic and easily available, and more interestingly, can thoroughly evaporate during the membrane formation process. As a result, an extra step for template removal is avoided.

Enhancement of Membrane Mechanical Properties. Polystyrene-based amphiphilic diblock copolymers (e.g., PS-*b*-PDMAEMA) are good candidates for membrane formation.[26,55] However, it is known that polystyrene films are fragile, especially for those films with highly porous structures.

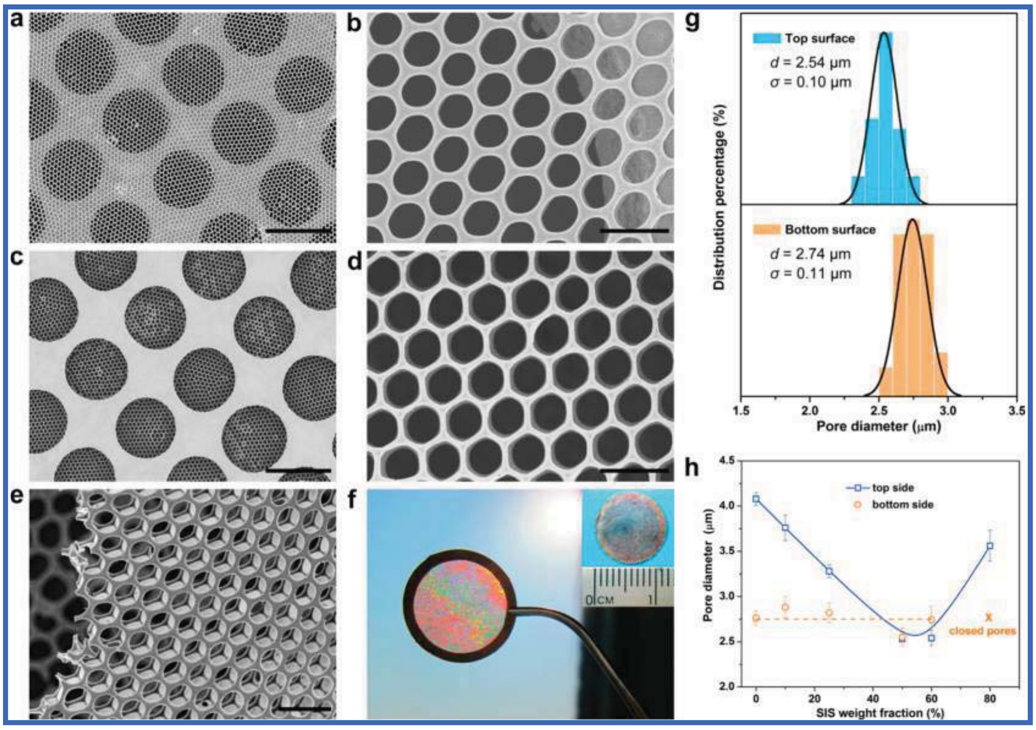

Figure 2. (a−e) SEM images of a typical perforated honeycomb composite membrane prepared by the transfer-free method from a blend of PS-*b*-PDMAEMA/SIS (60 wt % SIS). (a, b) Top side, (c, d) bottom side, and (e) cross-section. (f) Digital photographs of the composite membrane, the inset shows the actual dimension of the membrane. Scale bars: (a, c) 50 μm and (b, d, e) 5 μm. (g) Average pore diameter (*d*) of the top and bottom surfaces of a typical perforated honeycomb composite membrane prepared by the transfer-free method from a blend of PS-*b*-PDMAEMA/SIS (60 wt % SIS), and the corresponding standard deviations (σ). (h) Effects of SIS weight fractions in PS-*b*-PDMAEMA/SIS blends on the pore diameter.

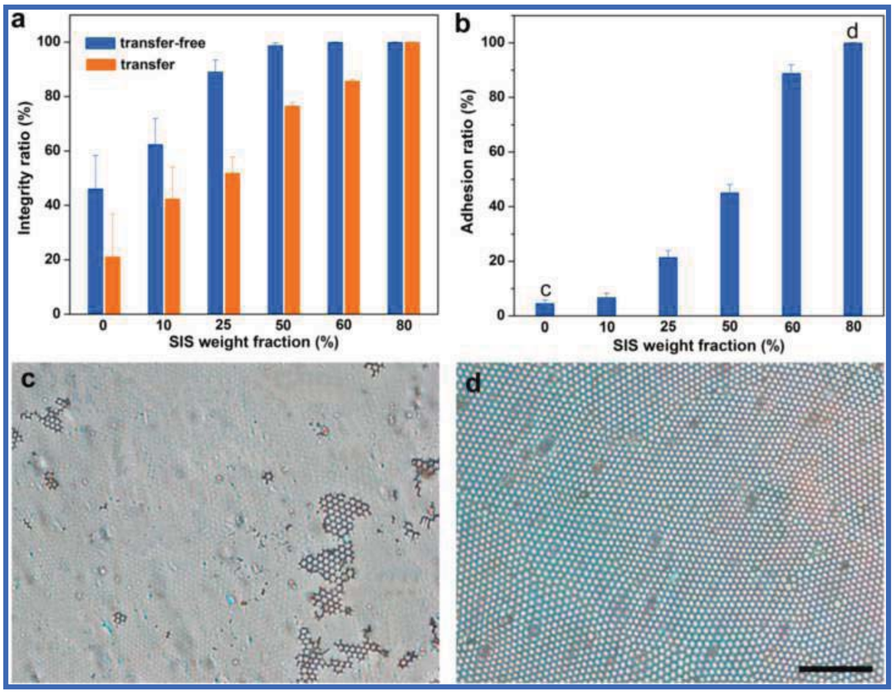

Figure 3. Membrane integrity and interfacial adhesion strength. (a, b) Effects of SIS weight fractions in PS-*b*-PDMAEMA/SIS blends on (a) the integrity and (b) the interfacial adhesion strength of the honeycomb membranes. (c, d) Typical optical images of residual pore structures of honeycomb membranes on supports after peeled off by a Scotch tape. (c) PS-*b*-PDMAEMA membrane and (d) PS-*b*-PDMAEMA/SIS blend (80 wt % SIS) membrane. Scale bar: 50 μm.

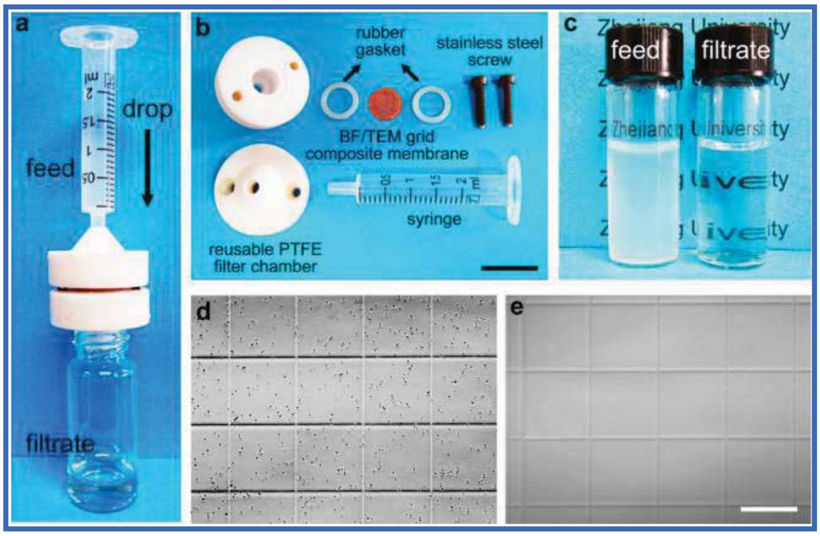

Figure 4. Yeast filtration. Digital photographs of (a) a typical yeast cell filtration process, (b) the membrane module used for cell separation, and (c) the feed and filtrate solutions. (d, e) Optical images of the (d) feed and (e) filtrate solutions on a hemocytometer. The feed solution in (a, c, d) has a yeast cell density of 3.4×10^6 cfu mL^{-1} (OD600 = 0.233) and the OD600 value of the filtrate is 0.001. Scale bars: (b) 20 mm and (d, e) 200 μm.

SIS is a commercially available elastomer and has been well demonstrated as an ideal material for constructing robust honeycomb films on nonplanar substrates.[57−59] Therefore, blends of PS-*b*-PDMAEMA and SIS with different compositions were investigated for the enhancement of membrane integrity and interfacial adhesion as well as pore structure control. As indicated in Figure 2h, the diameter of top surface pores of PS-*b*-PDMAEMA/SIS membranes can be tuned from 4.1 to 2.5 μm by changing the SIS weight fractions from 0 to 80 wt %, whereas the bottom pore size remains constant at about 2.7 μm, and dead-end pore structures are obtained at a high SIS ratio of 80 wt % (see the Supporting Information, Figures S2, S3). Besides, membranes containing 80 wt % SIS are sensitive to stretching and compressing, resulting in unstable and deformable pore structures at room temperature. A detailed discussion on the breath figure process for the formation of PS-*b*-PDMAEMA/SIS membranes can be found elsewhere (Supporting Information, breath figure process of PS-*b*-PDMAEMA/SIS membranes section and Figures S1−S7). Compared to the traditional transfer method, the integrity of the perforated honeycomb membranes has been significantly enhanced because of both the transfer-free method and the blending of elastic SIS (Figure 3a). Defects in the honeycomb composite membranes were evaluated through optical microscopy. The integrity ratio, which is the areal fraction of TEM grids covered by none-cracking honeycomb membranes increases with the weight fraction of SIS in the blends, and membranes prepared by the transfer-free method have obviously higher integrity ratios than those by the transfer method. Perforated honeycomb membranes with no cracks were obtained via the transfer-free method when the SIS weight fraction reaches 60%, whereas more than 15% area of the membrane prepared by the transfer method is still fractured (see the Supporting Information, Figures S8, S9). The elastic SIS can act as the strengthening phase in the as-prepared honeycomb membranes to protect pore structures from unexpected cracking in the self-adhesion, membrane drying, or separation processes.

The introduction of SIS can also enhance the adhesion strength between the honeycomb membrane and the porous support. Insufficient adhesion to supports leads to detachment of membranes from the supports,[55] which would obviously weaken or even eliminate the separation selectivity of the membranes. As far as we know, a direct and accurate measurement of the adhesion force of a thin polymeric membrane to a porous support is rather difficult. We evaluated the adhesion strength in a way that is borrowed from the evaluation of paint adhesion force. Perforated honeycomb membranes on supports were pressed by an adhesive Scotch tape onto the membrane surface. The adhesion strength is indicated via the adhesion ratio, which is defined as the ratio of the residual area to the whole area of membranes. As shown in Figure 3b, the adhesion ratio increases with the SIS fraction in the blends. The adhesion ratio of the membrane with 60 wt % SIS is nearly 20 times higher than that of the PS-*b*-PDMAEMA membrane. Figure 3c, d shows optical images of residual membranes with 0 and 80 wt % SIS, respectively. Almost all pore structures were removed from supports in the PS-*b*-PDMAEMA membranes, while the apparent membrane morphology in the membranes with 80 wt % SIS remains intact. Other typical images are shown in Figure S10 (Supporting Information). It can be concluded that the interfacial adhesion strength has been greatly improved by the introduction of elastic SIS. As a result of the improvement in membrane integrity and interfacial adhesion strength, the composite membrane can be preserved in dry state, unlike membranes reported previously that must be kept in wet state.[33−36] Membranes in the dry state are greatly beneficial for large scale production and practical applications.

Cell Separation. The honeycomb composite membranes were first applied to the filtration of yeast cells to evaluate the retention capability (Figure 4), which may provide a rapid and effective method to capture, enrich and even detect rare cells with ultralow concentration in a solution, e.g., *Cryptosporidium parvum* oocysts in the drinking water supply system[60] and circulating tumor cells in bloodstream.[61] The composite membrane with an outer diameter of 12 mm was mounted in a homemade permeation module, which consists of a syringe for holding the feedstock, a reusable polytetrafluoroethylene (PTFE) filter chamber, and rubber gaskets and stainless steel screws for membrane fixing and sealing (Figure 4b). This modified module could protect the composite membranes from possible damages in the mounting process and enable a working diameter of 8 mm. Yeast cells (*S. cerevisiae*) were dispersed in physiological saline with various cell densities from 3.2×10^5 to 3.4×10^6 cfu mL^{-1}, and the filtration was performed in a dead-end mode. It is noteworthy that the filtration could be carried out without external pressure, compared to the traditional microfiltration processes where 0.1 MPa or higher pressure is necessarily applied. The feed solution flowed through the filter chamber and the filtrate was collected for subsequent cell counting. This filtration process was recorded by a real-time monitoring optical video (see the Supporting Information, Movie S1). As expected, the filtration flux of the composite filters decreased with yeast cell density, and at least a flux of 3.0×10^2 L m^{-2} h^{-1} was achieved for a yeast cell density of 3.4×10^6 cfu mL^{-1}. Figure 4c−e shows typical digital photographs and cell counting results before and after the filtration by the membrane. The feed solution displayed a yeast cell density of 3.4×10^6 cfu mL^{-1} (OD600 = 0.233), whereas the filtrate showed nearly zero yeast cells (OD600 = 0.001). The filtration results demonstrated that almost 100% yeast cells were removed from the feed solution and a clear filtrate was obtained, which indicates perfect retention to cells with a larger size than the pore diameter. The excellent retention ability of the composite membranes stems from a narrow pore size distribution of the honeycomb membranes and an ultralow operation pressure of only several centimeters water. In addition, the filtration of yeast cells could also be performed via a sucking method (Figure 5). By carefully sucking the feed solution (OD600 = 0.233) in a vial into the syringe through a stainless steel needle, yeast cells would first pass through the porous supports and then be rejected by the honeycomb membranes, resulting in a clear filtrate solution (OD600 = 0.002) collected in the syringe (Figure 5b). The successful retention of yeast cells by this sucking method further indicates the improvement of the interfacial adhesion strength between the honeycomb membrane and the porous support, and the promising back flushing ability of the composite membranes.

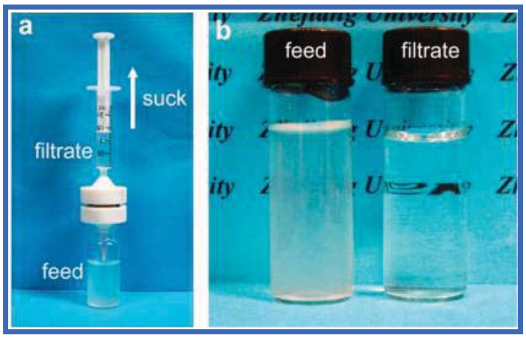

Figure 5. Digital photographs of (a) a typical yeast cell filtration via the sucking method and (b) the feed and filtrate solutions. The feed solution has a yeast cell density of 3.4×10^6 cfu mL^{-1} (OD600 = 0.233) and the OD600 value of the filtrate is 0.002.

Subsequently, the separation of cell mixtures of yeasts and lactobacilli (*S. thermophilus*) was investigated (Figure 6 and Supporting Information, Movie S2). It is known that the *S. cerevisiae* are elliptical cells with an average minor axis diameter of 3.1 μm and the *S. thermophilus* are spherical cells with an average diameter of 0.7 μm. Yeasts and lactobacilli were mixed and dispersed in physiological saline with various cell densities. The yeast density (D_Y) varied from 3.2×10^4 to 3.4×10^6 cfu mL^{-1} while the lactobacillus density (D_L) decreased from to 1.1×10^9 to 6.8×10^7 cfu mL^{-1}. The filtrate is still turbid because of the existence of lactobacilli although it seems slightly clearer than that of the feedstock of cell mixtures (Figure 6a). Figure 6b shows a typical SEM image of the mixed cells. As expected, yeast cells in the feed solution were almost completely retained by the aperture sieving effect of the honeycomb membranes, resulting in a permeation ratio of nearly zero (Figure 6d). Only lactobacilli can be observed from the SEM image of the filtrate (Figure 6c). Although several lactobacillus cells could link together to form a chain-like joint structure (Figure 6b) and enlarge the cell size, more than 70% of lactobacillus recovery was obtained in the filtrate (Figure 6d). The proportion of lactobacillus cells was observed to be significantly reduced in the filter residue (Supporting Information, Figure S11) as compared to that in the initial feed solution shown in Figure 6b. The filtration flux of cell mixtures is $\sim 2.6 \times 10^2$ L m^{-2} h^{-1}, which is slightly lower than that of the single solution of yeasts ($\sim 3.0 \times 10^2$ L m^{-2} h^{-1}).

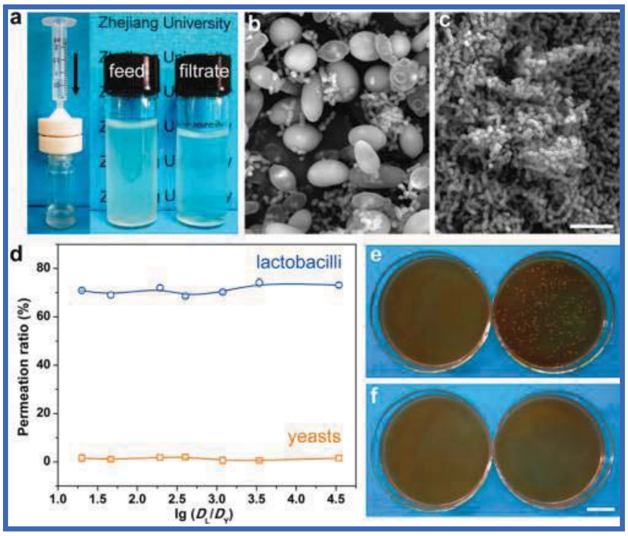

Figure 6. Cell separation. (a) Digital photographs of a typical separation process of the mixture of yeasts and lactobacilli, and the feed and filtrate solutions. (b, c) Typical SEM images of cells in the (b) feed and (c) filtrate solutions. The cell density of yeasts and lactobacilli in the feed solution was 3.4×10^6 and 6.8×10^7 cfu mL^{-1}, respectively. (d) Permeation ratios of yeasts and lactobacilli in the cell separation via the honeycomb composite membranes. (e, f) Digital photographs of the recultured filtrate solution in a lactobacillus growing medium (e) and yeast growing medium with 10 μg mL^{-1} erythromycin (f). The left culturing dishes in e and f were blank media as controls. Scale bars: (b, c) 5 μm and (e, f) 20 mm.

The diluted filtrate solution was recultured in a lactobacilli growing medium. The permeated lactobacillus cells show an excellent viability due to the free passage through the honeycomb composite membranes under an ultralow operation pressure (Figure 6e). It is important to perform cell separation at a low transmembrane pressure. For example, in the leukocyte depletion of blood, hemolysis would occur and leukocytes could be deformed and pushed through the pores under high pressures. Meanwhile, a yeast growing medium with 10 μg mL^{-1} erythromycin as the antibiotics was also used for reculturing the filtrate cells. As a result of the addition of erythromycin, the growth of lactobacillus cells would be completely suppressed without disturbing the breeding of yeast cells. The culturing results further indicate complete removal of yeast cells in the filtrate solution (Figure 6f). These results are consistent with those of yeast filtration shown in Figure 4 and 5. Therefore, it can be concluded that the perforated honeycomb composite membranes provide a high-resolution and energy-saving cell separation process.

4. CONCLUSION

In conclusion, we present a facile transfer-free strategy for the fabrication of robust perforated composite membranes with ordered and uniform pores. The strategy simplifies the procedures of fabricating composite membranes and greatly improves the homogeneity and interfacial adhesion strength of the membranes, enabling membranes that can be preserved in dry state and durable to back flushing. We demonstrated for the first time the use of a thin perforated membrane in high-resolution and energy-saving size-selective cell separation of yeasts and lactobacilli without external pressure. Almost 100% rejection of yeasts and more than 70% recovery of lactobacilli have been achieved by using a honeycomb membrane with an average pore diameter of 2.5 μm. In addition, the permeated lactobacilli show an excellent viability. This promising cell separation material may also be applied in other size-based separation systems, such as capture and detection of circulating tumor cells.

■ ASSOCIATED CONTENT

Ⓢ Supporting Information

Details of materials, instruments and characterization, the transfer fabrication method, membrane morphologies, solution viscosity, and surface chemistry analysis of membranes. This material is available free of charge via the Internet at http://pubs.acs.org.

■ AUTHOR INFORMATION

Corresponding Author

*E-mail: lswan@zju.edu.cn.

Notes

The authors declare no competing financial interest.

■ ACKNOWLEDGMENTS

This work is financially supported by the National Natural Science Foundation of China (Grants 51173161 and 21374100) and partially supported by the State Key Laboratory of Materials-Oriented Chemical Engineering (KL13-11).

■ REFERENCES

(1) Baker, R. W. *Membrane Technology and Applications*, 2nd ed.; John Wiley & Sons: New York, 2004.

(2) Adams, A. A.; Okagbare, P. I.; Feng, J.; Hupert, M. L.; Patterson, D.; Gottert, J.; McCarley, R. L.; Nikitopoulos, D.; Murphy, M. C.; Soper, S. A. Highly Efficient Circulating Tumor Cell Isolation from Whole Blood and Label-Free Enumeration Using Polymer-Based Microfluidics with an Integrated Conductivity Sensor. *J. Am. Chem. Soc.* **2008**, *130*, 8633−8641.

(3) Kaittanis, C.; Santra, S.; Perez, J. M. Role of Nanoparticle Valency in the Nondestructive Magnetic-Relaxation-Mediated Detection and Magnetic Isolation of Cells in Complex Media. *J. Am. Chem. Soc.* **2009**, *131*, 12780−12791.

(4) Wang, Y. Y.; Zhou, F.; Liu, X. L.; Yuan, L.; Li, D.; Wang, Y. W.; Chen, H. Aptamer-Modified Micro/Nanostructured Surfaces: Efficient Capture of Ramos Cells in Serum Environment. *ACS Appl. Mater. Interfaces* **2013**, *5*, 3816−3823.

(5) Zhang, P. H.; Cao, J. T.; Min, Q. H.; Zhu, J. J. Multi-Shell Structured Fluorescent-Magnetic Nanoprobe for Target Cell Imaging and on-Chip Sorting. *ACS Appl. Mater. Interfaces* **2013**, *5*, 7417−7424.

(6) Notta, F.; Doulatov, S.; Laurenti, E.; Poeppl, A.; Jurisica, I.; Dick, J. E. Isolation of Single Human Hematopoietic Stem Cells Capable of Long-Term Multilineage Engraftment. *Science* **2011**, *333*, 218−221.

(7) Drukker, M.; Tang, C.; Ardehali, R.; Rinkevich, Y.; Seita, J.; Lee, A. S.; Mosley, A. R.; Weissman, I. L.; Soen, Y. Isolation of Primitive Endoderm, Mesoderm, Vascular Endothelial and Trophoblast Progenitors from Human Pluripotent Stem Cells. *Nat. Biotechnol.* **2012**, *30*, 531−542.

(8) Kumamaru, H.; Ohkawa, Y.; Saiwai, H.; Yamada, H.; Kubota, K.; Kobayakawa, K.; Akashi, K.; Okano, H.; Iwamoto, Y.; Okada, S. Direct Isolation and Rna-Seq Reveal Environment-Dependent Properties of Engrafted Neural Stem/Progenitor Cells. *Nat. Commun.* **2012**, *3*, 1140.

(9) Avci, F. Y.; Li, X. M.; Tsuji, M.; Kasper, D. L. Isolation of Carbohydrate-Specific Cd4(+) T Cell Clones from Mice after Stimulation by Two Model Glycoconjugate Vaccines. *Nat. Protoc.* **2012**, *7*, 2180−2192.

(10) Yang, R. F.; Zheng, Y.; Burrows, M.; Liu, S. J.; Wei, Z.; Nace, A.; Guo, W.; Kumar, S.; Cotsarelis, G.; Xu, X. W. Generation of Folliculogenic Human Epithelial Stem Cells from Induced Pluripotent Stem Cells. *Nat. Commun.* **2014**, *5*, 3071.

(11) Griffiths, M. W. *Improving the Safety and Quality of Milk, Vol. 1: Milk Production and Processing*; Woodhead Publishing: Cambridge, U.K., 2010.

(12) Chrimes, A. F.; Khoshmanesh, K.; Stoddart, P. R.; Mitchell, A.; Kalantar-zadeh, K. Microfluidics and Raman Microscopy: Current Applications and Future Challenges. *Chem. Soc. Rev.* **2013**, *42*, 5880−5906.

(13) Tiwari, A.; Ramalingam, M.; Kobayashi, H.; Turner, A. P. F. *Biomedical Materials and Diagnostic Devices*; John Wiley & Sons: New York, 2012.

(14) He, D.; Susanto, H.; Ulbricht, M. Photo-Irradiation for Preparation, Modification and Stimulation of Polymeric Membranes. *Prog. Polym. Sci.* **2009**, *34*, 62−98.

(15) Yang, R.; Jang, H.; Stocker, R.; Gleason, K. K. Synergistic Prevention of Biofouling in Seawater Desalination by Zwitterionic Surfaces and Low-Level Chlorination. *Adv. Mater.* **2014**, *26*, 1711−1718.

(16) Warkiani, M. E.; Bhagat, A. A. S.; Khoo, B. L.; Han, J.; Lim, C. T.; Gong, H. Q.; Fane, A. G. Isoporous Micro/Nanoengineered Membranes. *ACS Nano* **2013**, *7*, 1882−1904.

(17) Wei, Q. H.; Bechinger, C.; Leiderer, P. Single-File Diffusion of Colloids in One-Dimensional Channels. *Science* **2000**, *287*, 625−627.

(18) Striemer, C. C.; Gaborski, T. R.; McGrath, J. L.; Fauchet, P. M. Charge- and Size-Based Separation of Macromolecules Using Ultrathin Silicon Membranes. *Nature* **2007**, *445*, 749−753.

(19) Dekker, C. Solid-State Nanopores. *Nat. Nanotechnol.* **2007**, *2*, 209−215.

(20) Zavala-Rivera, P.; Channon, K.; Nguyen, V.; Sivaniah, E.; Kabra, D.; Friend, R. H.; Nataraj, S. K.; Al-Muhtaseb, S. A.; Hexemer, A.; Calvo, M. E.; Miguez, H. Collective Osmotic Shock in Ordered Materials. *Nat. Mater.* **2012**, *11*, 53−57.

(21) Wang, Y.; Li, F. An Emerging Pore-Making Strategy: Confined Swelling-Induced Pore Generation in Block Copolymer Materials. *Adv. Mater.* **2011**, *23*, 2134−2148.

(22) Wu, D. C.; Xu, F.; Sun, B.; Fu, R. W.; He, H. K.; Matyjaszewski, K. Design and Preparation of Porous Polymers. *Chem. Rev.* **2012**, *112*, 3959−4015.

(23) van Rijn, P.; Tutus, M.; Kathrein, C.; Zhu, L.; Wessling, M.; Schwaneberg, U.; Boker, A. Challenges and Advances in the Field of Self-Assembled Membranes. *Chem. Soc. Rev.* **2013**, *42*, 6578−6592.

(24) Zhao, H.; Gu, W.; Thielke, M. W.; Sterner, E.; Tsai, T.; Russell, T. P.; Coughlin, E. B.; Theato, P. Functionalized Nanoporous Thin

Films and Fibers from Photocleavable Block Copolymers Featuring Activated Esters. *Macromolecules* **2013**, *46*, 5195−5201.

(25) Lee, W.; Ji, R.; Gosele, U.; Nielsch, K. Fast Fabrication of Long-Range Ordered Porous Alumina Membranes by Hard Anodization. *Nat. Mater.* **2006**, *5*, 741−747.

(26) Wan, L. S.; Li, J. W.; Ke, B. B.; Xu, Z. K. Ordered Microporous Membranes Templated by Breath Figures for Size-Selective Separation. *J. Am. Chem. Soc.* **2012**, *134*, 95−98.

(27) Peinemann, K. V.; Abetz, V.; Simon, P. F. Asymmetric Superstructure Formed in a Block Copolymer via Phase Separation. *Nat. Mater.* **2007**, *6*, 992−996.

(28) Nunes, S. P.; Sougrat, R.; Hooghan, B.; Anjum, D. H.; Behzad, A. R.; Zhao, L.; Pradeep, N.; Pinnau, I.; Vainio, U.; Peinemann, K. V. Ultraporous Films with Uniform Nanochannels by Block Copolymer Micelles Assembly. *Macromolecules* **2010**, *43*, 8079−8085.

(29) Nunes, S. P.; Behzad, A. R.; Hooghan, B.; Sougrat, R.; Karunakaran, M.; Pradeep, N.; Vainio, U.; Peinemann, K. V. Switchable Ph-Responsive Polymeric Membranes Prepared Via Block Copolymer Micelle Assembly. *ACS Nano* **2011**, *5*, 3516−3522.

(30) Qiu, X.; Yu, H.; Karunakaran, M.; Pradeep, N.; Nunes, S. P.; Peinemann, K.-V. Selective Separation of Similarly Sized Proteins with Tunable Nanoporous Block Copolymer Membranes. *ACS Nano* **2012**, *7*, 768−776.

(31) Marques, D. S.; Vainio, U.; Chaparro, N. M.; Calo, V. M.; Bezahd, A. R.; Pitera, J. W.; Peinemann, K. V.; Nunes, S. P. Self-Assembly in Casting Solutions of Block Copolymer Membranes. *Soft Matter* **2013**, *9*, 5557−5564.

(32) Yu, H.; Qiu, X.; Nunes, S. P.; Peinemann, K.-V. Self-Assembled Isoporous Block Copolymer Membranes with Tuned Pore Sizes. *Angew. Chem., Int. Ed.* **2014**, *53*, 10072−10076.

(33) Yang, S. Y.; Ryu, I.; Kim, H. Y.; Kim, J. K.; Jang, S. K.; Russell, T. P. Nanoporous Membranes with Ultrahigh Selectivity and Flux for the Filtration of Viruses. *Adv. Mater.* **2006**, *18*, 709−712.

(34) Yang, S. Y.; Park, J.; Yoon, J.; Ree, M.; Jang, S. K.; Kim, J. K. Virus Filtration Membranes Prepared from Nanoporous Block Copolymers with Good Dimensional Stability under High Pressures and Excellent Solvent Resistance. *Adv. Funct. Mater.* **2008**, *18*, 1371−1377.

(35) Jackson, E. A.; Hillmyer, M. A. Nanoporous Membranes Derived from Block Copolymers: From Drug Delivery to Water Filtration. *ACS Nano* **2010**, *4*, 3548−3553.

(36) Jeon, G.; Jee, M.; Yang, S. Y.; Lee, B. Y.; Jang, S. K.; Kim, J. K. Hierarchically Self-Organized Monolithic Nanoporous Membrane for Excellent Virus Enrichment. *ACS Appl. Mater. Interfaces* **2014**, *6*, 1200−1206.

(37) Ke, B. B.; Wan, L. S.; Chen, P. C.; Zhang, L. Y.; Xu, Z. K. Tunable Assembly of Nanoparticles on Patterned Porous Film. *Langmuir* **2010**, *26*, 15982−15988.

(38) Widawski, G.; Rawiso, M.; Francois, B. Self-Organized Honeycomb Morphology of Star-Polymer Polystyrene Films. *Nature* **1994**, *369*, 387−389.

(39) Bai, H.; Du, C.; Zhang, A. J.; Li, L. Breath Figure Arrays: Unconventional Fabrications, Functionalizations, and Applications. *Angew. Chem., Int. Ed.* **2013**, *52*, 12240−12255.

(40) Muñoz-Bonilla, A.; Fernández-García, M.; Rodríguez-Hernández, J. Towards Hierarchically Ordered Functional Porous Polymeric Surfaces Prepared by the Breath Figures Approach. *Prog. Polym. Sci.* **2014**, *39*, 510−554.

(41) Wan, L. S.; Zhu, L. W.; Ou, Y.; Xu, Z. K. Multiple Interfaces in Self-Assembled Breath Figures. *Chem. Commun.* **2014**, *50*, 4024−4039.

(42) Wan, L. S.; Li, Q. L.; Chen, P. C.; Xu, Z. K. Patterned Biocatalytic Films via One-Step Self-Assembly. *Chem. Commun.* **2012**, *48*, 4417−4419.

(43) Wan, L. S.; Ke, B. B.; Zhang, J.; Xu, Z. K. Pore Shape of Honeycomb-Patterned Films: Modulation and Interfacial Behavior. *J. Phys. Chem. B* **2012**, *116*, 40−47.

(44) Zhu, L. W.; Yang, W.; Ou, Y.; Wan, L. S.; Xu, Z. K. Synthesis of Polystyrene with Cyclic, Ionized and Neutralized End Groups and the Self-Assemblies Templated by Breath Figures. *Polym. Chem.* **2014**, *5*, 3666−3672.

(45) Zhu, L. W.; Ou, Y.; Wan, L. S.; Xu, Z. K. Polystyrenes with Hydrophilic End Groups: Synthesis, Characterization, and Effects on the Self-Assembly of Breath Figure Arrays. *J. Phys. Chem. B* **2014**, *118*, 845−854.

(46) Zhu, L. W.; Wu, B. H.; Wan, L. S.; Xu, Z. K. Polystyrene with Hydrophobic End Groups: Synthesis, Kinetics, Interfacial Activity, and Self-Assemblies Templated by Breath Figures. *Polym. Chem.* **2014**, *5*, 4311−4320.

(47) Zhu, L. W.; Yang, W.; Wan, L. S.; Xu, Z. K. Synthesis of Core Cross-Linked Star Polystyrene with Functional End Groups and Self-Assemblies Templated by Breath Figures. *Polym. Chem.* **2014**, *5*, 5175−5182.

(48) Govor, L. V.; Bashmakov, I. A.; Kiebooms, R.; Dyakonov, V.; Parisi, J. Self-Organized Networks Based on Conjugated Polymers. *Adv. Mater.* **2001**, *13*, 588−591.

(49) Nishikawa, T.; Ookura, R.; Nishida, J.; Arai, K.; Hayashi, J.; Kurono, N.; Sawadaishi, T.; Hara, M.; Shimomura, M. Fabrication of Honeycomb Film of an Amphiphilic Copolymer at the Air-Water Interface. *Langmuir* **2002**, *18*, 5734−5740.

(50) Hayakawa, T.; Horiuchi, S. From Angstroms to Micrometers: Self-Organized Hierarchical Structure within a Polymer Film. *Angew. Chem., Int. Ed.* **2003**, *42*, 2285−2289.

(51) Ma, H.; Cui, J.; Song, A.; Hao, J. Fabrication of Freestanding Honeycomb Films with through-Pore Structures via Air/Water Interfacial Self-Assembly. *Chem. Commun.* **2011**, *47*, 1154−1156.

(52) Cong, H.; Wang, J.; Yu, B.; Tang, J. Preparation of a Highly Permeable Ordered Porous Microfiltration Membrane of Brominated Poly(Phenylene Oxide) on an Ice Substrate by the Breath Figure Method. *Soft Matter* **2012**, *8*, 8835−8839.

(53) Yin, S. Y.; Goldovsky, Y.; Herzberg, M.; Liu, L.; Sun, H.; Zhang, Y. Y.; Meng, F. B.; Cao, X. B.; Sun, D. D.; Chen, H. Y.; Kushmaro, A.; Chen, X. D. Functional Free-Standing Graphene Honeycomb Films. *Adv. Funct. Mater.* **2013**, *23*, 2972−2978.

(54) Zhang, C.; Wang, X.; Min, K.; Lee, D.; Wei, C.; Schulhauser, H.; Gao, H. Developing Porous Honeycomb Films Using Miktoarm Star Copolymers and Exploring Their Application in Particle Separation. *Macromol. Rapid Commun.* **2014**, *35*, 221−227.

(55) Ou, Y.; Zhu, L. W.; Xiao, W. D.; Yang, H. C.; Jiang, Q. J.; Li, X.; Lu, J. G.; Wan, L. S.; Xu, Z. K. Nonlithographic Fabrication of Nanostructured Micropatterns via Breath Figures and Solution Growth. *J. Phys. Chem. C* **2014**, *118*, 4403−4409.

(56) Yan, F.; Ding, A.; Girones, M.; Lammertink, R. G.; Wessling, M.; Borger, L.; Vilsmeier, K.; Goedel, W. A. Hierarchically Structured Assembly of Polymer Microsieves, Made by a Combination of Phase Separation Micromolding and Float-Casting. *Adv. Mater.* **2012**, *24*, 1551−1557.

(57) Li, L.; Zhong, Y.; Gong, J.; Li, J.; Chen, C.; Zeng, B.; Ma, Z. Constructing Robust 3-Dimensionally Conformal Micropatterns: Vulcanization of Honeycomb Structured Polymeric Films. *Soft Matter* **2011**, *7*, 546−552.

(58) Li, L.; Zhong, Y.; Gong, J.; Li, J.; Huang, J.; Ma, Z. Fabrication of Robust Micro-Patterned Polymeric Films via Static Breath-Figure Process and Vulcanization. *J. Colloid Interface Sci.* **2011**, *354*, 758−764.

(59) Du, C.; Zhang, A.; Bai, H.; Li, L. Robust Microsieves with Excellent Solvent Resistance: Cross-Linkage of Perforated Polymer Films with Honeycomb Structure. *ACS Macro Lett.* **2013**, *2*, 27−30.

(60) Warkiani, M. E.; Chen, L. Q.; Lou, C. P.; Liu, H. B.; Zhang, R.; Gong, H. Q. Capturing and Recovering of Cryptosporidium Parvum Oocysts with Polymeric Micro-Fabricated Filter. *J. Membr. Sci.* **2011**, *369*, 560−568.

(61) Hosokawa, M.; Hayata, T.; Fukuda, Y.; Arakaki, A.; Yoshino, T.; Tanaka, T.; Matsunaga, T. Size-Selective Microcavity Array for Rapid and Efficient Detection of Circulating Tumor Cells. *Anal. Chem.* **2010**, *82*, 6629−6635.